

**SYNTHESIS OF TiO₂ NANOWIRE ARRAYS AND THEIR APPLICATIONS
FOR ORGANIC SOLAR CELLS**

**MS. WITCHAYA ARPAVATE
ID: 56300700509**

**A THESIS SUBMITTED AS A PART OF THE REQUIREMENTS
FOR THE DEGREE OF MASTER OF ENGINEERING
IN ENERGY TECHNOLOGY AND MANAGEMENT**

**THE JOINT GRADUATE SCHOOL OF ENERGY AND ENVIRONMENT
AT KING MONGKUT'S UNIVERSITY OF TECHNOLOGY THONBURI**

2ND SEMESTER 2014

COPYRIGHT OF THE JOINT GRADUATE SCHOOL OF ENERGY AND ENVIRONMENT

Synthesis of TiO₂ Nanowire Arrays and Their Applications for Organic Solar Cells

Ms. Witchaya Arpavate

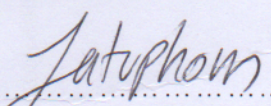
ID: 56300700509

A Thesis Submitted as a Part of the Requirements
for the Degree of Master of Engineering
in Energy Technology and Management

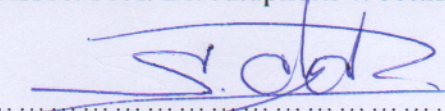
The Joint Graduate School of Energy and Environment
at King Mongkut's University of Technology Thonburi

2nd Semester 2014

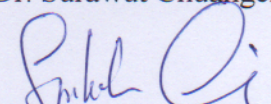
Thesis Committee


.....
(Assoc. Prof. Dr. Jatuphorn Wootthikanokkhan)


Advisor


.....
(Dr. Surawut Chuangchote)

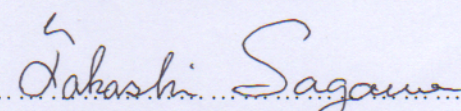
Co-Advisor


.....
(Asst. Prof. Dr. Siriluk Chiarakorn)

Member


.....
(Dr. Pisist Kumnorkaew)

Member


.....
(Prof. Dr. Takashi Sagawa)

External Examiner

Thesis Title: Synthesis of TiO₂ Nanowire Arrays and Their Applications for Organic Solar Cells

Student's name, organization and telephone/fax numbers/email

Miss Witchaya Arpavate
The Joint Graduate School of Energy and Environment (JGSEE)
King Mongkut's University of Technology Thonburi (KMUTT)
126 Pracha Uthit Rd., Bangmod, Tungkru, Bangkok 10140 Thailand
Telephone: 08-6393-1058
Email: june_dbsg@hotmail.com

Supervisor's name, organization and telephone/fax numbers/email

Assoc. Prof. Dr. Jatuphorn Wootthikanokkhan
School of Energy, Environment and Materials
Division of Materials Technology
King Mongkut's University of Technology Thonburi (KMUTT)
126 Pracha Uthit Rd., Bangmod, Tungkru, Bangkok 10140 Thailand
Telephone: 0-2470-8693-99 Ext. 316
Fax: 0-2427-9062
E-mail Address: jatuphorn.woo@kmutt.ac.th

Co-Advisor's name, organization and telephone/fax numbers/email

Dr. Surawut Chuangchote
The Joint Graduate School of Energy and Environment (JGSEE)
King Mongkut's University of Technology Thonburi (KMUTT)
126 Pracha Uthit Rd., Bangmod, Tungkru, Bangkok 10140 Thailand
Telephone: 08-6388-0493
Fax: 0-2872-6978
E-mail: surawut.chu@kmutt.ac.th

Topic: Synthesis of TiO₂ Nanowire Arrays and Their Applications for Organic Solar Cells

Name of Student: Miss Witchaya Arpavate

Student ID: 56300700509

Name of Supervisor: Assoc. Prof. Dr. Jatuphorn Wootthikanokkhan

Name of Co-Advisor: Dr. Surawut Chuangchote

ABSTRACT

Organic photovoltaic cells (OPVs), especially polymer-based devices called polymer photovoltaic cells, have recently received a great attention due to the simple process and the lower and reasonable production costs compared with silicon-based solar cells. However, the efficiencies of organic photovoltaic cells are still very low compared with inorganic photovoltaic cells. There are different metal oxides that are generally used in hybrid solar cells as electron acceptor. TiO₂ is one of the attractive choices for electron acceptor materials in this solar cell due to its high electron mobility, high chemical stability, and suitable band gap. In this work, ZnO nanorod arrays were synthesized by a hydrothermal method and used as templates for the fabrication of TiO₂ nanotubes. The obtained TiO₂ nanowires were investigated by scanning electron microscopy (SEM) and X-ray diffraction (XRD). It was observed that density and alignment of nanowire arrays could be varied by preparation conditions. SEM images showed that the morphologies of TiO₂ nanowire arrays were corresponding to the ZnO nanorods templates. Various surface modifications of ZnO nanorods and TiO₂ nanotubes, including the addition of a layer of TiO₂ nanofilm, addition of TiO₂ nanoparticles, and TiCl₄ treatment, were studied. For fabrication of hybrid photovoltaic cells, the blended 6,6-phenyl-C₆₁-butyric acid methylester (PCBM) and poly(3-hexylthiophene) (P3HT) were coated on the obtained TiO₂ nanowires and the electrode was deposited by thermal evaporation. Surface-modified nanowires were applied as an electron transporting layer in hybrid photovoltaic cells for higher cell efficiencies. Photovoltaic properties and power conversion efficiency of devices made of TiO₂ nanowire arrays were investigated.

Keywords: TiO₂, Nanowires, Hybrid photovoltaic cell, Surface modification, ZnO nanorods

ACKNOWLEDGEMENTS

I would like to express thanks to my thesis advisor, Assoc. Prof. Dr. Jatuphorn Wootthikanokkhan, for his invaluable suggestions and constant support throughout this thesis. I would also like to acknowledge Dr. Surawut Chuangchote for his good advice for solving many problems in my experiments, not only guidance for research but also writing skill and thesis presentation. I would not have achieved this far and my thesis would not have been completed without his support. He always encourages and stands by me throughout my study in master degree. I would like to acknowledge Prof. Dr. Takashi Sagawa (Sagawa sensei) for guiding me during my exchange research in Japan. Although I had been in Japan for short period, 3 months, he treated me like his official students. He supported my researches by allowing me to use all instruments in his laboratory. I also would like to thanks Sagawa sensei for being an external examiner. Thank you for warm welcome, friendly environment in laboratory and new great experiences in Japan. Moreover, I would like to thanks my other committee members, Asst. Prof. Dr. Siriluk Chiarakorn and Dr. Pisist Kumnorkaew for their helpful suggestions and comments during my research.

I would like to acknowledge the financial support of the Joint Graduate School of Energy and Environment (JGSEE), King Mongkut's University of Technology Thonburi.

Finally, I most appreciatively acknowledge my beloved family and my friends for all their support throughout the period of the research.

CONTENTS

CHAPTER	TITLE	PAGE
	ABSTRACT	i
	ACKNOWLEDGEMENTS	ii
	CONTENTS	iii
	LIST OF TABLES	v
	LIST OF FIGURES	vi
1	INTRODUCTION	
	1.1 Rationale	1
	1.2 Literature Review	2
	1.3 Research Objectives	9
	1.4 Scopes of Research Work	10
2	THEORIES	
	2.1 Organic-inorganic Solar Cells (hybrid solar cells)	11
	2.2 Device Structure	11
	2.3 Working Principles of Device	13
	2.4 Performance Characteristics	14
	2.5 TiO ₂ as Electron Transporting Layer	15
	2.6 Fabrication of TiO ₂ Nanotubes (Nanowires)	17
3	METHODOLOGY	
	3.1 Preparation of Metal Oxide Nanowires	20
	3.2 Surface Modifications of Metal Oxide Nanowire	21
	3.3 Characterizations of Metal Oxide Nanowires	23
	3.4 Fabrication of Organic Solar Cells	23
	3.5 Photovoltaic Characterizations	24
4	RESULTS AND DISCUSSION	
	4.1 Effects of Preparation Conditions on Size and Morphology of ZnO Nanorods	25
	4.2 Photovoltaic Characterizations of Hybrid Photovoltaic Devices Made of ZnO Nanorods	30
	4.3 Fabrication of TiO ₂ Nanotubes by Using ZnO Nanorods as Templates	32

CONTENTS_(Cont')

CHAPTER	TITLE	PAGE
	4.4 Surface Modifications of Metal Oxides Nanowires	33
	4.5 Photovoltaic Characterizations of Hybrid Photovoltaic Devices Made of TiO ₂ Nanowires	37
5	CONCLUSION	45
	REFERENCES	46

LIST OF TABLES

TABLES	TITLE	PAGE
1.1	Comparisons of power conversion efficiencies (PCE) of photovoltaic cells made of TiO ₂ nanostructures under different surface modification of TiO ₂ .	9
4.1	Photovoltaic characteristic properties of cells made of ZnO nanorods arrays grown on ZnO seeds at different seed layers	31
4.2	Photovoltaic characteristic properties of cells made of metal oxides	39
4.3	Photovoltaic characteristic properties of cells made of TiO ₂ with and without vacuum-assisted coating of active layer	43
4.4	Photovoltaic characteristic properties of cells made of ZnO nanorods with and without vacuum-assisted coating of active layer	44

LIST OF FIGURES

FIGURES	TITLE	PAGE
1.1	Schematic diagram of preparing ZnO rod arrays on the glass substrate.	3
1.2	Schematic for the growth mechanism of nanowires with different thicknesses of seed layers.	3
1.3	Schematic illustration of the growth mechanism model of the ZnO nanorods at different reaction temperatures.	4
1.4	Schematic model for effect of seed layer thickness on alignment and diameter of nanorods.	5
2.1	Schematic diagram of (i) bilayer heterojunction and (ii) bulk heterojunction photoactive layers.	12
2.2	Structure and working principles of bulk heterojunction hybrid solar cell.	13
2.3	Energy levels and the harvesting of energy from a photon for an acceptor/donor interface within a hybrid polymer/nanoparticle solar cell.	14
2.4	Current density–voltage (J–V) characteristics for a generic illuminated solar cell. This indicates the three major device characteristics which determine PCE.	15
2.5	Blend of various semiconductors in nano-architectures and conducting polymer films in solar cell. (a) nanoparticles; (b) nanorods; (c) nano-tetrapods; (d) conducting polymer immersed in porous semiconductor nano-network; (e) nanorods arrays; and (f) nanotube arrays	16
2.6	A comparison of the electron pathways through (a) nanoparticles, (b) randomized and (c) oriented nanotubular structured TiO ₂	17
2.7	Schematic of the steps for forming the end-closed TiO ₂ nanotube	19
3.1	Flow chart showing the step for preparation of seeded substrate	20
3.2	Steps of surface modification	21
3.3	Energy level of devices made of TiO ₂ nanowires	23

LIST OF FIGURES (Cont')

FIGURES	TITLE	PAGE
4.1	SEM images of ZnO nanorod arrays grown on various seed layer thicknesses: (a) 1, (b) 2, and (c) 3 seed layer(s)	25
4.2	XRD patterns of (a) cleaned substrate, (b) ZnO seeded on substrate, and (c) ZnO nanorod arrays on coated substrate	26
4.3	SEM images of ZnO nanorod arrays grown on seeded substrates at different times of hydrothermal growth: (a) 10, (b) 20, (c) 30, and (d) 40 min	28
4.4	SEM images of ZnO nanorod arrays grown on seeded substrates at different temperatures of hydrothermal growth: (a) 25, (b) 90, (c) 120, and (d) 130 °C	29
4.5	SEM images of ZnO nanorods grown on with different cooling styles after annealing step: (a) fast cooling style and (b) slow cooling style	30
4.6	Cell structure of hybrid photovoltaic cells made of ZnO nanorods	30
4.7	<i>J-V</i> curves of hybrid photovoltaic cells made of ZnO nanorods grown on ZnO seed at different seeding thickness	31
4.8	SEM images of (a) ZnO nanorods as templates for producing (b) TiO ₂ nanotubes	32
4.9	EDX spectra of (a) ZnO nanorods as templates for producing (b) TiO ₂ nanotubes	33
4.10	SEM images of unmodified ZnO nanorod arrays in (a) top view and (b) cross-sectional view.	34
4.11	SEM images of modified surface of ZnO nanorods: (a) unmodified ZnO nanorods, (b) TiO ₂ nanofilms on ZnO surfaces, (c) TiO ₂ nanoparticles on ZnO surfaces and (d) TiCl ₄ treatment on ZnO nanorods	35
4.12	SEM images in cross-sectional view of (a) TiO ₂ nanofilms on ZnO surfaces and (b) TiO ₂ nanoparticles on ZnO surfaces	35
4.13	EDX spectra of modified surface of ZnO by addition of TiO ₂ nanoparticles	36

LIST OF FIGURES (Cont')

FIGURES	TITLE	PAGE
4.14	SEM images of TiO ₂ nanotubes with surface modification: (a) unmodified TiO ₂ nanotubes in top view, (b) unmodified TiO ₂ nanotubes in cross-sectional view, and (c) TiCl ₄ treatment on TiO ₂ nanotubes	37
4.15	Device structure of hybrid photovoltaic cell made of metal oxides	37
4.16	<i>J-V</i> characteristics of hybrid photovoltaic devices fabricated from metal oxides	38
4.17	IPCE characteristics of hybrid photovoltaic devices fabricated from metal oxides	40
4.18	SEM images of cells before and after improvement of performance by vacuum-assisted coating: (a) cell made of TiO ₂ nanofilms before improvement, (b) cell made of TiO ₂ nanofilms after improvement, (c) cell made of TiO ₂ nanotubes before improvement, and (d) cell made of TiO ₂ nanotubes after improvment	42
4.19	<i>J-V</i> characteristics of hybrid photovoltaic devices fabricated from TiO ₂ nanofilms and nanotubes with and without improvement of active layer coating	43
4.20	<i>J-V</i> characteristics of hybrid photovoltaic devices fabricated from ZnO nanorods with and without vacuum-assisted coating of active layer	44

CHAPTER 1

INTRODUCTION

1.1 Rationale

Organic solar cells or organic photovoltaic cells (OPVs), one type of the solar cells, are the devices produce electricity from solar energy directly. Organic photovoltaic cells, especially polymer-based devices, called polymer photovoltaic cells, have recently received great attention due to the simple process and the lower and reasonable production costs when compared to that of the silicon-based solar cells. The absorber layer has conjugated low band gap polymer as electron donor that is blended with a second material (electron acceptor) to achieve a layer as called bulk heterojunction. In organic solar cells, electron donor material absorbs sunlight or photons to generate excitons. When excitons move to the interface of the two bulk components, they dissociate into electrons and holes. After separation, electrons move to the acceptor material and are carried to the cathode and holes are carried to the anode. In the case of OPVs which are focused on regioregular poly(3-hexylthiophene) (P3HT, as donor) and 6,6-phenyl-C₆₁-butyric acid methylester (PCBM, as acceptor), their high efficiencies have been reported 4-5% [1, 2, 3]. However the efficiencies of OPVs are still very low, as compared to those of the inorganic photovoltaic cells. Organic solar cells have not only low efficiencies, but also low strength, low stability and low mobility to transfer the excited electrons or the holes. Recently, in order to overcome the low mobility of carriers and improve the cell efficiencies, hybrid solar cells which combined organic materials as donor and inorganic material as acceptors have been studied [4, 5, 6].

Various kinds of inorganic semiconductors that are fabricated in the form of one-dimensional (1D) nanostructures have been researched in hybrid solar cells because of their high charge mobility [5, 7]. Among the different metal oxides that are used in hybrid solar cells as electron acceptor, such as CdSe, TiO₂, ZnO, and so on. TiO₂ is one of the attractive electron acceptors due to its high electron mobility, high chemical stability and suitable band gap [4, 8]. There are many methods to synthesize TiO₂ nanotubes, including sol-gel process, atomic layer deposition, electrochemical anodic oxidation, hydrothermal treatment and liquid phase deposition (LPD) [8, 9, 10].

Among the various techniques to fabricate TiO₂ one-dimensional nanostructure, a template-assisted method with liquid phase deposition is a simple technique that can operate at low temperature and ambient pressure without requiring special equipment or substrates. ZnO nanorod arrays are synthesized by hydrothermal method and used as template for fabrication of TiO₂ nanotubes [4, 11, 12]. Liquid phase deposition method can be adjusted to grow long and dense nanotubes, which is totally different from other reported works. The TiO₂ nanotubes are developed to align vertically on the conducting glass substrates in an array form and applied as an electron transporting layer in organic photovoltaic cells for higher cell efficiencies.

1.2 Literature Review

1.2.1 Preparation of ZnO Nanorods

M. Guo *et al.* [13] fabricated well-aligned ZnO nanorod arrays by using the hydrothermal method and studied the effects of the growth conditions that were substrate's pre-treatment, growth temperature, deposition time and the concentration of the precursors. Pre-treatment of substrates with annealing had great influence on nanorod diameter and alignment of ZnO nanorod arrays. The deposition temperature had little effect on rod orientation, but it had great effect on the aspect ratio and the photoluminescent of nanorods. The concentration of precursors can rather impact the rod diameter and its distribution. The growth time was explained by the kinetic studies: the nanorods tend to be short and wide with a fast step within the first hour and they were long rods with high aspect ratio in a slow step.

M. Guo *et al.* [14] studied the effects of hydrothermal growth temperature to control the diameter and orientation of ZnO nanorod arrays. Average diameters of nanorods were approximately 30-70 nm. Well-aligned ZnO nanorod arrays were used in Grätzel-type solar cell and the high photoconversion efficiency is about 2.4% when the deposition temperature is 95 °C.

J. Zhao *et al.* [15] synthesized ZnO nanorods on ZnO-coated seed surfaces by a hydrothermal method using Zn(NO₃)₂/NaOH solution. The average diameter of nanorods increased slightly when concentration of precursor increased. The optimal temperature for the maximum growth rate at any given Zn²⁺ ion concentration increased with concentration of Zn²⁺. The growth rate of nanorods decreased with the deposition time. Adding PEG into

solution for coating on the seed surfaces resulted in high density and large sizes of crystallites, which became densely packed and thick ZnO nanorods those were perpendicular to the substrates.

M. Yang *et al.* [16] investigated the preparatory conditions, such as seed layers, precursor concentration and reaction time. The glass substrate was immersed in an aqueous solution to form seed layers. The result showed that ZnO seed layers were required for the good alignment of ZnO rod arrays. The average length of rods was approximately 2-3 μm that was controlled by concentration of precursors and reaction time. With increasing reaction time, ZnO rod arrays density increased while the diameter of rods was invariable.

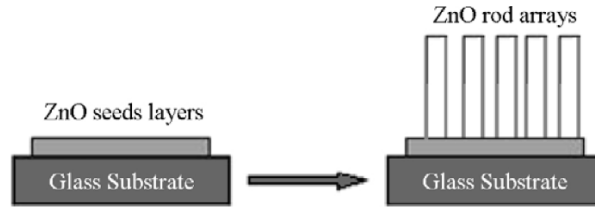


Fig. 1.1 Schematic diagram of preparing ZnO rod arrays on the glass substrate [16].

L.W. Ji *et al.* [17] studied the thickness of seed layers that had an influence on the vertically well-aligned ZnO nanowire arrays. The nanowire diameter was increased in a range from 50 nm to 130 nm and density of nanowire was decreased from 110 nm to 60 nm with increasing ZnO seed layer thickness. In this paper, sputtering technique was used to control the layer thickness. The results showed that thicker seed layers gave well-aligned ZnO nanowires while thinner layers gave poor-aligned ZnO nanowire arrays.

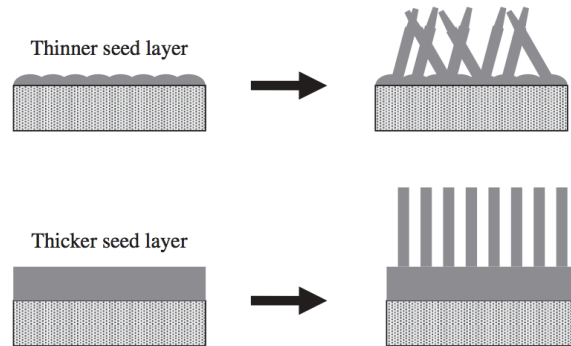


Fig. 1.2 Schematic for the growth mechanism of nanowires with different thicknesses of seed layers [17].

Z. Qin *et al.* [18] synthesized ZnO nanorod arrays by using a low-temperature hydrothermal method under different reaction temperature. ZnO nanorods growth rate increased with increasing deposition temperature. ZnO nanorod arrays had a better vertical alignment with increasing growth temperature. Well-aligned ZnO nanorod arrays were applied to DSSCs and the power conversion efficiency was 0.31%.

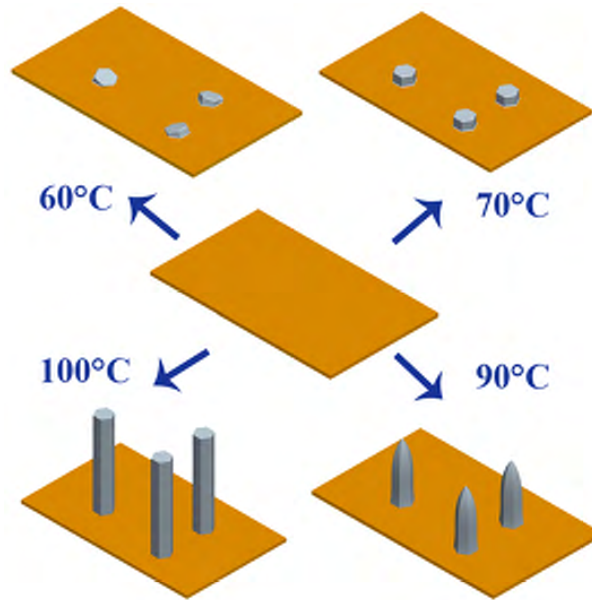


Fig. 1.3 Schematic illustration of the growth mechanism model of the ZnO nanorods at different reaction temperatures [18].

S.-N. Bai *et al.* [19] studied the effects of a solution concentration that was coated on the Si substrate by the sol-gel technique. The solution concentration used as ZnO seed-layer films was varied in a range from 0.05 M to 1.2 M. The roughness, grain size, and crystallinity of the ZnO films increased with the concentration of solution increasing. In this study, the optimum solution concentration for preparing ZnO seed-layer films was 1.0 M. Moreover the results showed that ZnO seed films could be a parameter to control the well-aligned ZnO nanowires.

H. Ghayour *et al.* [20] studied the influence of seed layer thickness on the orientation of ZnO nanorods. ZnO seed layer thickness was varied from 20 nm to 320 nm and fabricated on Si substrate by sputtering method. The growth temperature of ZnO nanorods was 95°C and the reaction time was 2 h. The results showed that the rod length increased and the diameter of nanorods decreased with decreasing seed layer thickness. The alignment of nanorods depended on roughness frequency, crystallinity and grain size.

Therefore, the seed layer thickness played an important role in the nanorod orientation. With increasing seed layer thickness, the roughness frequency was lower, crystallinity was higher and grain size was larger. The well-aligned ZnO nanorods were grown on thicker seed layer while the poor alignment of ZnO nanorods was grown on thinner seed layer.

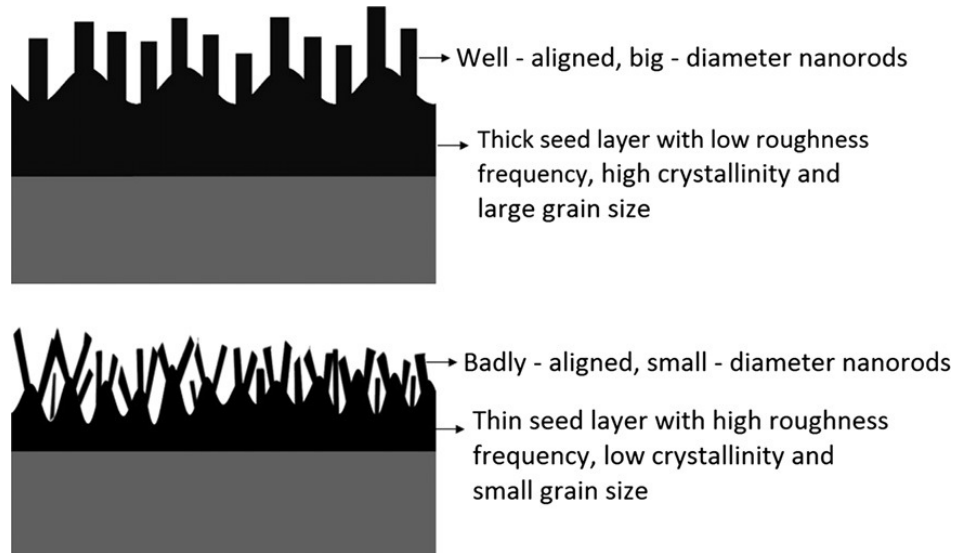


Fig. 1.4 Schematic model for effect of seed layer thickness on alignment and diameter of nanorods [20].

K. A. Wahid *et al.* [21] synthesized ZnO nanorod structures by using the hydrothermal method to study the effect of seed annealing temperature and growth time. ZnO seed layer was coated on SiO₂ substrates by spin-coating technique and annealed at different temperature in a range from 100°C to 200°C for 1h. The maximum length and diameter of ZnO nanorods were obtained at annealing temperature of 150°C. The growth duration was varied from 3 to 9 h. The size of ZnO nanorods increased with growth time. The seed annealing temperature and deposition time had great influences on the size of ZnO nanorods.

J. Deng *et al.* [22] studied the concentration of seed precursor and the pretreatment duration of ZnO seeds. The zinc acetate precursor was used to coat on ITO substrate at different concentration, there are 5, 15 and 25 mM. The pretreatment time was varied from 8, 16 and 24 min. The density of ZnO nanowires increased with seed precursor concentration and pretreatment time increasing. The rod diameter obviously increased with

the increase of pretreatment time.

M. Wang *et al.* [23] investigated the effects of seed layers, ZnO colloid concentrations, substrates and precursor concentrations, which were preparatory parameters to control the alignment of the ZnO nanorod arrays. The nanorods that grew on seed-coated substrate were higher density and better vertical alignment than ZnO nanorods from bare substrate. The colloid concentration for ZnO seed layer could be the effective role to control the growth alignment of nanorods. When ZnO colloid concentration increased from 0.05 to 1 M., ZnO nanorod arrays were better orientation and the distribution range of deviation angle narrows decreased. The results demonstrated that ZnO nanorods on seed-coated FTO substrate were better alignment than that on seed-coated Si substrate. Precursor concentration had an insignificant influence on the well-aligned ZnO nanorod arrays. The alignment of nanorods could be improved with precursor concentration increasing; the concentration of precursor was varied from 0.005 M to 1 M. However, the vertical alignment percentage constant of ZnO nanorod alignment was almost stable when the precursor concentration increased to 1 M. It could be concluded when the precursor had high enough concentration, further increase of precursor concentration had no obvious help to the alignment of arrays.

X. Dong *et al.* [24] fabricated ZnO nanorod arrays on glass substrates that had been coated by the electrospinning technique to produce a seed layer. The time of electrospinning coating had a great role to control the density of ZnO nanorod arrays. When the coating time was extended, ZnO nanorod density increased and well-aligned nanorod was obtained.

1.2.2 Preparation of TiO₂ Nanowires

J. Jitputti *et al.* [25] used a low-temperature hydrothermal method to produce flower-like titanate superstructure with 250-450 nm in diameter. The experimental results showed that temperature had a great impact on the product structure when the titanate nanosheets were calcined at 500 °C, their structures converted into anatase TiO₂ and their specific surface area decreased. The amount of H₂ evolved from water splitting reaction was investigated as photocatalytic activity measurement that showed the flower-like titanate superstructure had a high photocatalytic activity. Furthermore, the photocatalytic activity of anatase TiO₂ was higher than commercial TiO₂ anatase powder.

S.A. Berhe *et al.* [26] synthesized rutile TiO₂ nanorods by the hydrothermal method with new seeding conditions, which were manganese oxyhydroxide (MnOOH)

nanoparticles and a sheet of TiO_2 . The seed layers played an effective role in controlling the growth of rutile TiO_2 nanorods when compared to the rutile nanorods from bare substrates. The results demonstrated that rods had diameter of 20 nm and their length grew up to 2 μm without bundling under condition of low precursor concentration while rod fusion could occur at high precursor concentration and long growth time. The efficiency of photovoltaic cells using the rutile TiO_2 nanorod films depended on the size of bundling and rod length. From this research, the rutile TiO_2 nanorods could be synthesized by hydrothermal method directly, but rutile TiO_2 was not suitable for photovoltaic cells when compared with anatase phase TiO_2 .

J.-H. Lee *et al.* [11] fabricated aligned TiO_2 one-dimensional nanostructured arrays by using ZnO nanorods as templates with the liquid deposition method. Synthesis of TiO_2 nanotubes in anatase phase was limited that was the anatase TiO_2 could not be synthesized directly, then ZnO nanorod templates were used in this work. The results showed that the different thickness of TiO_2 nanotubes could be controlled by deposition time. Furthermore, the preparation method, which was the idea of selective etching and deposition, could also be applied to other one-dimensional nanostructured oxide materials and this method was expected to find widespread applications.

1.2.3 Surface Modification of TiO_2

T. Rattanaavoravipa *et al.* [4] prepared TiO_2 nanotube arrays on the substrate through one-step liquid phase deposition technique and improved the efficiency of hybrid photovoltaic cell by modifying the surface of TiO_2 nanotubes with N719 ruthenium dye. The obtained results demonstrated that the surface modification of TiO_2 had improved the power conversion efficiency in term of the enhancement of electron injection. Unmodified cell had a power conversion efficiency of 0.02%, which was lower than 0.065% of the modified cell efficiency.

Z.J. Wang *et al.* [27] modified TiO_2 nanotubes with dye (N719) and applied them to hybrid bulk heterojunction solar cells to compare with the pristine polymer solar cells, the hybrid solar cells with active layer of TiO_2 nanoparticles, non-modified TiO_2 nanotubes and dye modified TiO_2 nanotubes. The experimental results show that the power conversion efficiency of photovoltaic cell based on dye modified TiO_2 nanotubes was better than the others.

J. Lui *et al.* [28] produced TiO_2 nanorods by the hydrolysis of titanium tetrakisopropoxide (TTIP) using oleic acid (99%) as a surfactant at low temperatures and

studied the effects of surface ligands on the exciton dissociation and the charge transport in hybrid solar cells by modifying TiO₂ nanorods with different ligands, which were oleic acid (OLA), n-octyl-phosphonic acid (OPA) and thiophenol (TP). The consequences showed that the power conversion efficiency of cell could be improved obviously by modifying TiO₂ nanorods with thiophenol than oleic acid and n-octyl-phosphonic acid. Moreover, all the results proved that thiophenol is the best ligand for fabricating hybrid photovoltaic cells based on TiO₂ nanorods.

M.-C. Wu *et al.* [29] fabricated hybrid photovoltaic devices based on anatase TiO₂ nanorods and modified the surface area of TiO₂ by adding polymethylmethacrylate (PMMA) to smoothen the film surface, reduce the occurrence of air pores and defects, and enhance light absorption. The optimized photovoltaic cell with 1.6 wt% PMMA concentration has a better device efficiency than the other experimental results.

M.-S. Wu *et al.* [30] studied the surface modification of porous TiO₂ photoanodes by using anodic electrochemical deposition in an aqueous TiCl₃ electrolyte. The surface modification of mesoporous TiO₂ photoanode was an effective way to improve the efficiency of DSSC (dye-sensitized solar cell) that increased the short-circuit density and decreased the dark current density. The photoelectron conversion efficiency of DSSC was higher than DSSCs with bare and TiCl₄-treated TiO₂ photoanodes.

S. H. Kang *et al.* [31] synthesized anatase TiO₂ nanotubes by anodic oxidation on a pure titanium substrate and applied TiO₂ nanotubes as a working electrode in a solid-state dye-sensitized solar cell. To improve open-circuit voltage and cell performance, the ZnO shell was coated on the TiO₂ nanotubes and hydrogen peroxide treatment was used to improve the fill factor by reducing the thickness of the TiO₂ barrier layer. Thus, the surface modification of TiO₂ by covering the thin ZnO layer increased the power conversion efficiency of dye-sensitized TiO₂ solar cells.

S.-C. Choi *et al.* [32] modified the surface of light scattering TiO₂ particles with dual-coated with Al₂O₃ and SiO₂ nanoparticles in the dye-sensitized solar cell (DSSC). The surface treatment used the colloidal alumina and the colloidal silica as surface coating precursors. Al₂O₃ and SiO₂ nanoparticles were coated on the light scattering TiO₂ particles by the sol-gel method. The dual-coated light scattering TiO₂ layer could increase short-circuit photocurrent of DSSC device and caused the increasing of cell performance.

Table 1.1 Comparisons of power conversion efficiencies (PCE) of photovoltaic cells made of TiO₂ nanostructures under different surface modifications of TiO₂.

Application	Semiconductor	Modified Treatment	PCE (%)	Ref.
Hybrid solar cell	TiO ₂ nanotubes	Unmodified	0.02	[4]
		N719 dye	0.656	[4]
		Unmodified	0.0603	[27]
		N719 dye	0.0805	[27]
	TiO ₂ nanorods	Unmodified	0.096	[28]
		Thiophenol	0.157	[28]
		Unmodified	0.47	[29]
		1.6 %wt polymethylmethacrylate	0.65	[29]
DSSC	TiO ₂ nanotubes	Unmodified	0.578	[31]
		ZnO coating	0.704	[31]
		H ₂ O ₂ treatment	0.640	[31]
		ZnO coating and H ₂ O ₂ treatment	0.906	[31]
	TiO ₂ nanoparticles	Unmodified	5.32	[32]
		Al ₂ O ₃ and SiO ₂ coating	6.14	[32]

1.3 Research Objectives

1. To fabricate TiO₂ nanowire arrays with good physical, optical and electronic properties from a solution process, *i.e.* hydrothermal method and liquid phase deposition.
2. To improve the surface area and properties of metal oxide nanowires on the conducting glass substrates.
3. To develop efficient organic solar cells composed of metal oxide nanowire arrays with high power conversion efficiency and stability.

1.4 Scopes of Research Work

In this research, I have fabricated nanowire arrays in the form of nanorods or nanotubes from metal oxides, i.e. ZnO and/or TiO₂.

ZnO nanorods have been fabricated by the sol-gel technique and hydrothermal method under various conditions. The influence of solution concentration and thickness of seed layer has been studied.

Various methods to modify the surface of the ZnO nanorods have been studied. The interesting modifications are: (1) growing of TiO₂ nanotubes by liquid deposition using ZnO nanorods as templates; (2) adding of TiO₂ nanofilms on the surface of ZnO nanorods; (3) adding of nanoparticles on the surface of ZnO nanorods; and (4) treatment of nanowire surface by TiCl₄.

The ZnO nanorods and TiO₂ nanotubes have been characterized by a scanning electron microscope (SEM) and an X-ray diffractometer (XRD). Obtained metal oxide nanowires have been used as electron transporting layer in the hybrid organic solar cells.

CHAPTER 2

THEORIES

2.1 Organic-Inorganic Solar Cells (Hybrid Solar Cells)

Solar cells are a great option for renewable energy and have attracted much interest to solve the increase in world energy consumption. Silicon-based solar cells, the first generation of devices, are the most dominant in the solar energy market and have been reported power conversion efficiencies of up to 25%. Although silicon solar cells have high performances, the production costs of devices are still expensive. The development of solar cells to reduce the price lead to the second generation of solar cells those are made of semiconductor materials such as copper indium gallium selenide (CIGS) and cadmium telluride (CdTe) in the form of thin film cells. However, the thin film solar cells are lower manufacturing costs than silicon solar cells, they have some disadvantages such as rare element (indium) or toxic material (cadmium) [33, 34, 35, 36, 37]. The discovery of organic materials solves the previous problems of high production costs and limited and poisonous materials and results in the third generation solar cells, which are organic solar cells, but they have some drawbacks such as low performance and low mobility of carriers. To develop the power conversion efficiencies of the cells, researchers combine both organic and inorganic materials to take the advantages of their properties. The combination devices are called “Organic-inorganic hybrid solar cells”, which have organic material as donor and inorganic semiconductor in form of nanostructures (particles, rods, film, tubes, *etc.*) as acceptor. Moreover, hybrid solar cells are recently gaining the attention because of simple process, low-cost production and more flexible devices than the other solar cells [5,36, 37, 38].

2.2 Device Structure

The structure of a hybrid solar cell is composed of a photoactive layer and two electrodes that have different work roles. The anode, as a high work function, is a semitransparent oxide layer, its function is to allow light to pass through and to transfer electron back to the cells, usually indium tin oxide (ITO) or fluorine doped tin oxide (FTO) which is a transparent electrode widely used in optoelectronics such as solar cells and light

emitting diodes. It coats on the top of a flexible plastic or transparent substrate (glass). The cathode is a thin metal such as aluminum (Al), calcium (Ca) or magnesium (Mg). Its work role is to collect electrons from the device [5, 36, 39].

The photoactive layer is sandwiched between two electrodes and there are two different structure types. The first type is a bilayer structure, which contains two different layers of a polymer and an inorganic material that are completely separated from each other, and it makes single interface area for electron transportation. The second type is bulk heterojunction structure, which consists of organic and inorganic semiconductor as donor and acceptor material respectively and they are blended together for increasing the interface area to transfer electron [4, 36, 39, 40].

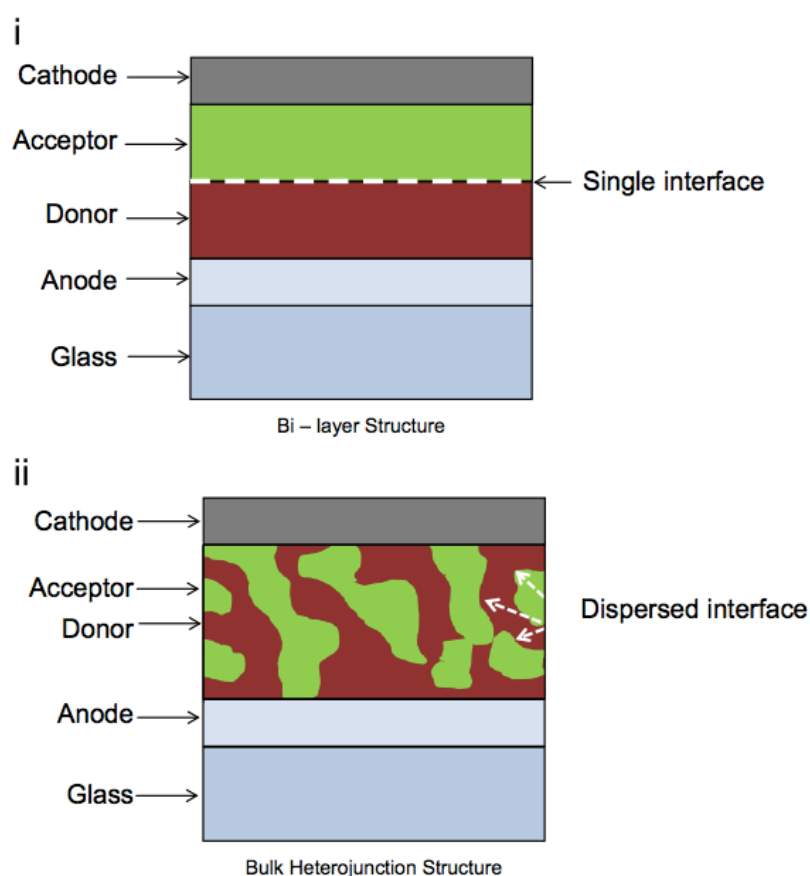


Fig. Schematic diagram of (i) bilayer heterojunction and (ii) bulk heterojunction photoactive layers [36].

2.3 Working Principles of Device

In the system of the hybrid solar cells, there are multiple steps to convert light into electricity. The sunlight or photons are absorbed by the donor material. The electrons in the valence band (VB) are excited to the conduction band (CB) and attracted to holes by Coulomb interaction these are called “excitons”. The excitons (bound electron–hole pairs) are generated in donor material and diffuse to the interface of the two bulk components, they dissociate into free electrons and holes. After separation, the charges are moved by the internal electric field, the acceptor material receives the electrons and transfers to the cathode electrode for charge collection while the holes remain within the donor material and are collected at the anode [4, 5, 36, 39].

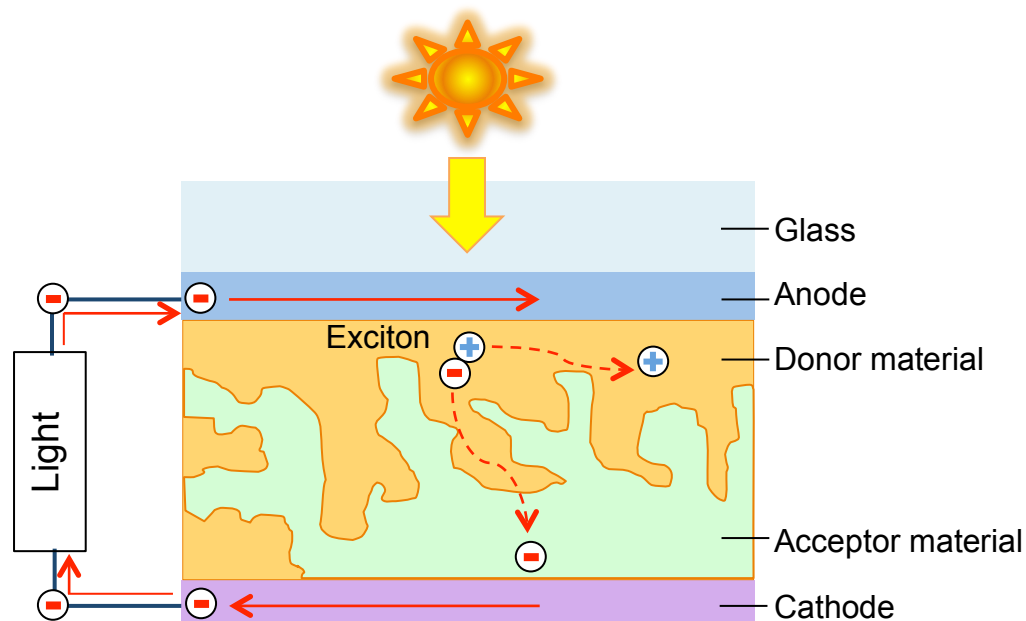


Fig. 2.2 Structure and working principles of bulk heterojunction hybrid solar cell.

The energy that is required to dissociate excitons, is greater than the lowest unoccupied molecular orbital (LUMO) of the donor and the conduction band of the acceptor. Then electrons hop to the acceptor material. Mostly, the highest occupied molecular orbital (HOMO) of donor is higher than the valence band of acceptor, but less than the photoanode energy level to certify holes in the donor material move to the anode

electrode. The energy levels of the photoactive layer and the electrodes have a great influence on charge collection yield [34, 41].

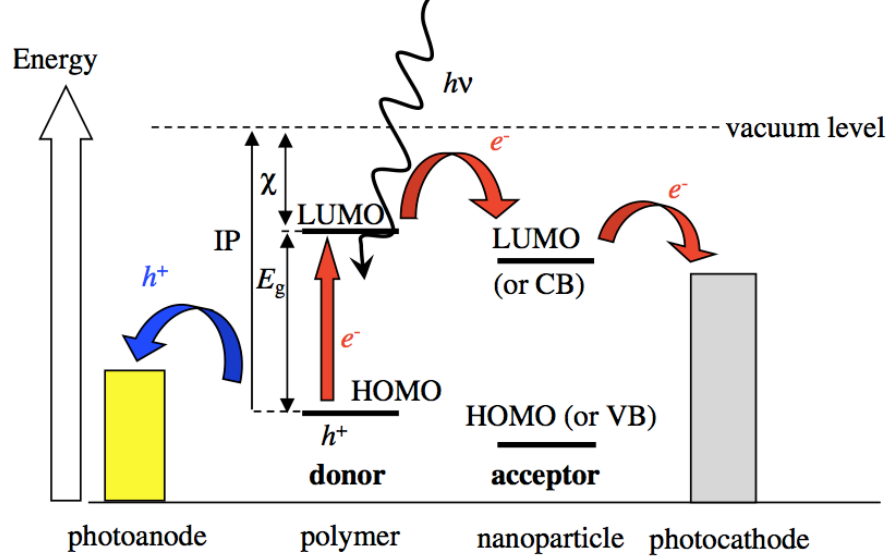


Fig. 2.3 Energy levels and the harvesting of energy from a photon for an acceptor/donor interface within a hybrid polymer/nanoparticle solar cell [41].

2.4 Performance Characteristics

The photovoltaic efficiency of solar cells is the ratio between the electrical output that are converted by devices and the input of solar energy that the devices can absorb. The power conversion efficiency (PCE) of a solar cell is calculated by the following equation:

$$PCE = \frac{J_{sc} \cdot V_{oc} \cdot FF}{P_{in}} \quad (1)$$

where J_{sc} is the short circuit current density (A/cm^2), V_{oc} is the open circuit voltage (V), FF is the fill factor and P_{in} is the incident light power density. For comparison of solar cell efficiency, the standard light input power is used at $1000 W/m^2$ ($100 mW/cm^2$), which is incident spectrum of AM 1.5 G and has the incident angle of 48.2° on the earth's surface.

The fill factor is the ratio of the maximum power from the device to the product of the short circuit current density and the open circuit voltage. Its practical value is less than the ideal value of 1. FF is a measure of squareness of the J-V curve that is largest rectangular area under the curve.

$$FF = \frac{J_m \cdot V_m}{J_{sc} \cdot V_{oc}} \quad (2)$$

where J_m and V_m are the maximum power point current density and voltage.

There are 3 major parameters; J_{sc} , V_{oc} , and FF; that determine the photovoltaic efficiency of a solar cell [36, 40].

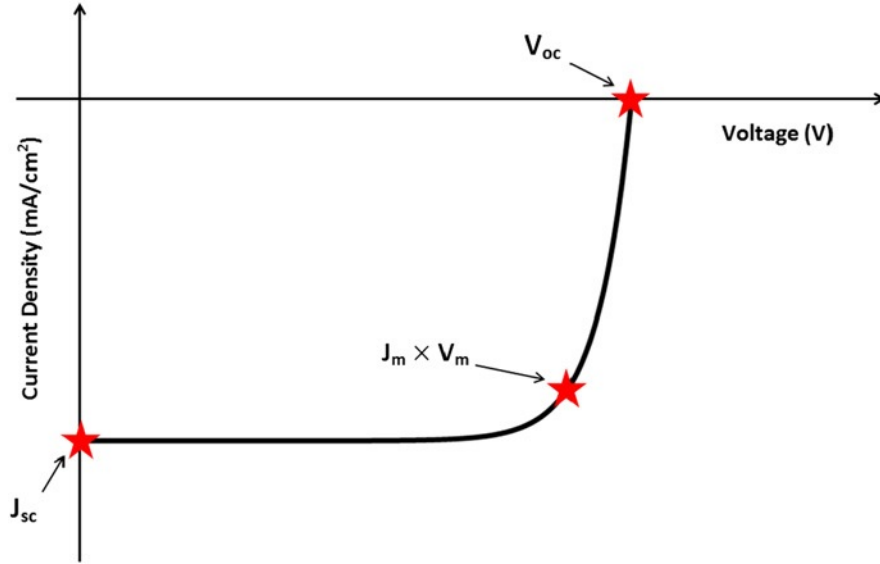


Fig. 2.4 Current density–voltage (J–V) characteristics for a generic illuminated solar cell. This indicates the three major device characteristics that determine PCE [36].

2.5 TiO₂ as Electron Transporting Layer

Inorganic semiconductors have been attracted as an electron transporting layer in hybrid solar cells to improvement the cell's efficiency because of their electronic properties, such as a high dielectric constant, a high charge mobility and thermal stability. Most materials, which have been studied, are metal oxides that include SnO₂, TiO₂, and ZnO. These semiconductors are able to form in vertical alignment, which have been synthesized in nanostructures. There are various types of nanostructures such as nanoparticles, nanorods, nano-tetrapods, nanotubes, nanowires, nanobelts and porous network. It should be noted that (1) nanorod is a material in the form of rod in nanoscale, (2) nanotube is a material in similar form but it is hollow material, (3) nanowire can be

both nanorod and nanotube or other shapes that have properties of charge conductivity [4, 9, 36]. Although the comparison of cell performance based on the ZnO and TiO₂ nanostructures is still controversial, TiO₂ is an interesting material of several metal oxides due to its high electron mobility, high chemical stability and appropriate band gap to use in solar cells for photovoltaic performance. TiO₂ is a wide-band gap semiconductor with 3.0 eV for rutile, 3.2 eV for anatase. Anatase phase TiO₂ is preferred for optoelectronic applications rather than rutile phase TiO₂ because electron transport of anatase TiO₂ is better than rutile and anatase TiO₂ has reduced charge carrier recombination [4, 5, 8, 10, 36, 43].

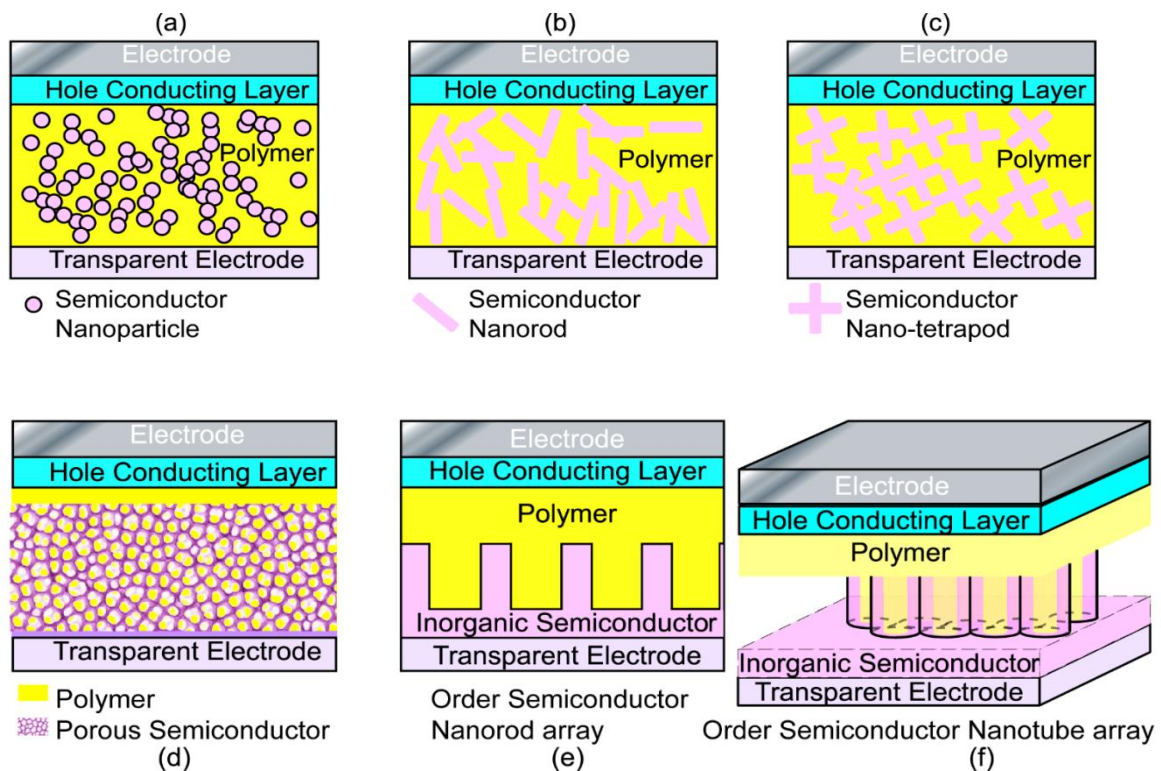


Fig. 2.5 Blend of various semiconductors in nano-architectures and conducting polymer films in solar cell: (a) nanoparticles; (b) nanorods; (c) nano-tetrapods; (d) conducting polymer immersed in porous semiconductor nano-network; (e) nanorods arrays; and (f) nanotube arrays [42].

In order to improve overall cell efficiencies, one-dimensional (1D) nanostructures of TiO₂ have been widely used as electron transporting layers for increasing the interface

area between inorganic and organic materials, and the effective charge transport pathways. The drawback of TiO_2 nanoparticles is the limited transportation of photo-excited electrons, because of low electron diffusion coefficient and the scattering effect of free electrons such as electron trapped sites at defects, surfaces and grain boundaries between nanoparticles. Therefore, charge collection efficiency is reduced owing to the increase of charge recombination at the trapping sites. The nanotube of TiO_2 provides unique properties of high aspect ratio which include large surface area, highly oriented crystallinity, high cation exchangeability, easier separation and recyclability. However, randomized TiO_2 nanotubes can suppress the possibility of charge recombination, Both of TiO_2 nanoparticles and disordered TiO_2 nanotubes have long electron pathways. Besides, the cells made of TiO_2 nanotubes are better performance than that of the nanorods based system due to larger interface areas [42, 43].

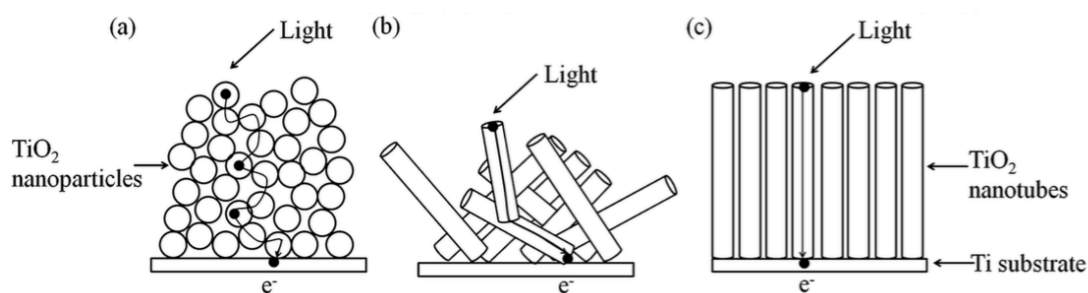


Fig. 2.6 A comparison of the electron pathways through (a) nanoparticles, (b) randomized and (c) oriented nanotubular structured TiO_2 [43]

The ordered TiO_2 nanotube arrays are supposed to achieve higher efficiency of charge collection due to fast electron pathways with minimum charge recombination site. Furthermore, the TiO_2 nanotubes are often more desirable for applications in photovoltaic cells, sensing, catalysis, and photocatalysis [11, 43].

2.6 Fabrication of TiO_2 Nanotubes (Nanowires)

TiO_2 nanotubes have been synthesized by many preparation methods, such as the anodic oxidation method, hydrothermal method, and liquid phase deposition (LPD) method. Anodic oxidation, which is an electrochemical method, can produce ordered alignment of TiO_2 nanotubes with high aspect ratio (length-to-diameter ratio) and

controllable size, but this process has disadvantages that include difficult separation of TiO_2 array film from substrates, limited of mass production, expensive cost of fabrication equipment and environmental concern about the use of highly toxic solvents. Hydrothermal method is common process to manufacture TiO_2 nanotubes in large amount because of simple way to achieve nanotubes, feasible for extensive applications and environmental friendly method. However, this technique needs a long reaction time and is difficult to obtain uniform size of nanotubes [9,43-44]. Liquid phase deposition is a soft chemical method to produce metal oxide thin films from an aqueous solution of precursor metal species that is hydrolyzed by scavenged solvent such as boric acid, metal oxide films occur and grow directly at the surface of substrate. This process has no requirement of high temperature and vacuum system [45, 46, 47].

Generally, TiO_2 nanotubes can be fabricated by the anodic oxidation method. On the other hand, LPD with ZnO as a template is also able to prepare TiO_2 nanotubes conveniently and easily. In case of wet process, well-aligned ZnO nanorod arrays can be prepared by low temperature hydrothermal method, they are template-free, and they have potential for scale-up. LPD has been developed for the fabrication of metal oxide thin films by simply immersing the substrate in the precursor aqueous solution that is a metal-fluoro complex, which is hydrolyzed by adding fluoride scavenger such as boric acid. Addition of solvent shifts this chemical equilibrium of hydrolysis and drives precipitation of the oxide. Because this preparation depends on chemical equilibrium of between a metal-fluoro complex and metal oxide, homogeneous oxide films can be deposited on several types of substrates with large areas. LPD has better control of the hydrolysis reaction and of the supersaturation of solution as compared with the other wet processes. The deposition of TiO_2 nanotubes and the selective-etching of ZnO nanorod template move on at the same time through the careful control of process parameters. Moreover, TiO_2 one-dimensional nanostructure arrays, which are obtained by the immersion of substrate, could be controlled by different deposition time [11, 46, 47].

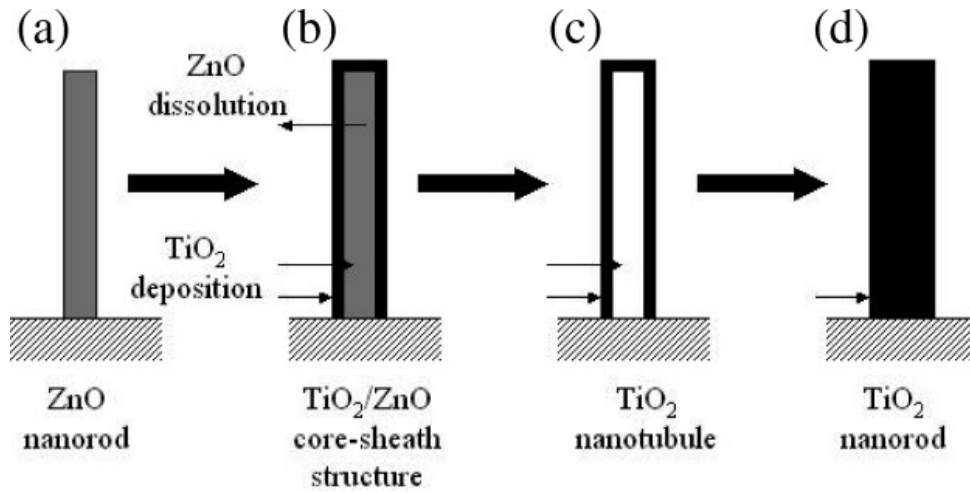


Fig. 2.7. Schematic of the steps for forming the end-closed TiO_2 nanotube [11].

The LPD is a very simple and attractive technique to create various metal oxide films for researchers because no vacuum, no high temperature, no expensive equipment and no special substrates are required. Therefore, LPD has effective production costs and environmental friendly impact. Moreover, The development of LPD technique has released a way for the preparation of organic-inorganic hybrid material [12, 46, 47].

CHAPTER 3

METHODOLOGY

3.1 Preparation of Metal Oxide Nanowires

3.1.1 Synthesis of ZnO Nanorods

ZnO nanorod arrays were prepared vertically on fluorine-doped tin oxide (FTO) glass substrate to be the template for TiO₂ nanotubes by the hydrothermal method at low temperatures. It should be noted that FTO could have been more suitable than indium tin oxide (ITO) for use as a substrate because the decomposition temperature of the ITO substrate was 450 °C, which was the condition of calcination to form the electron-transporting layer. Firstly, zinc acetate was dissolved in ethanol at concentration of 0.01 M, which served as seed coating solution and FTO substrate was cleaned ultrasonically in distilled water, ethanol and acetone, respectively. Before seeding, the cleaned FTO substrate was treated by UV ozone killer for 30 min. Then the seed precursor was dropped onto FTO substrate by spin-coating technique and the coated substrate was annealed in an electrical furnace at 260 °C for 5 h in the air. Preparation of seed surface was shown in Fig 3.1. After the heat treatment, ZnO nanorods were grown perpendicularly from seed layer by immersing ZnO-coated glass substrate into Zn(NO₃)₂ (0.04 M) and NaOH (0.8 M) at 110 °C for 20 min. Subsequently, the FTO substrate with aligned ZnO nanorod arrays were washed by distilled water to remove the unreacted residues and dried in ambient air.

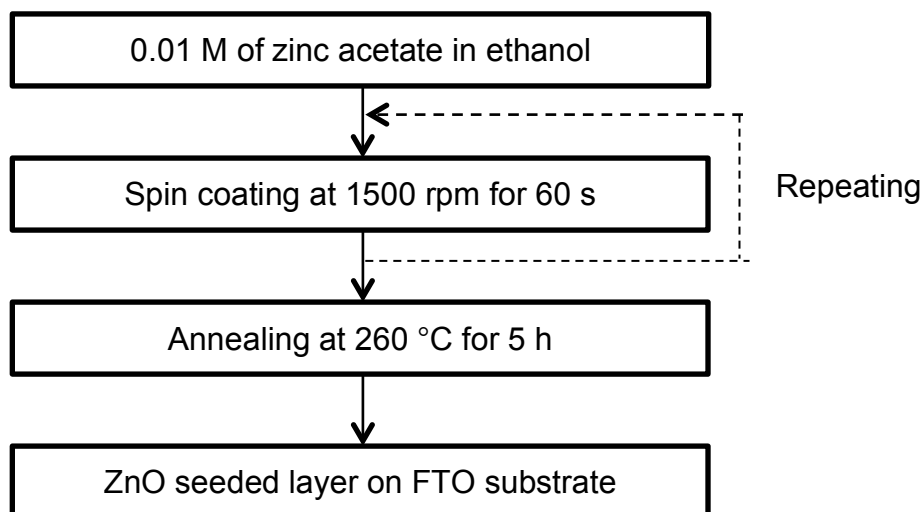


Fig. 3.1 Flow chart showing the step for preparation of seeded substrate.

3.1.2 Synthesis of TiO₂ Nanotubes

After the preparation of well-aligned ZnO nanorod arrays, TiO₂ materials were deposited on the ZnO nanorod arrays by liquid phase deposition. Ammonium hexafluorotitanate (NH₄)₂TiF₆ was dissolved in distilled water at 0.05 M and boric acid (H₃BO₃) was prepared at concentration of 0.15 M, both of them served as treatment aqueous solution. The ZnO nanorod templates on FTO glass substrate were immersed into mixed aqueous solution at room temperature for 3 h and the substrate was posed perpendicular with the bottom of bottle. Then the obtained TiO₂ nanotube arrays on the glass substrate were thoroughly washed by distilled water to eliminate any residual solution.

3.2 Surface Modifications of Metal Oxide Nanowires

ZnO nanorods were successfully fabricated by the hydrothermal method. The first surface treatment of ZnO nanorods is change of ZnO to be TiO₂ in the form of nanotubes by liquid phase deposition method as described above. Other surface modifications those were carried out in this research are addition of TiO₂ nanofilms, addition of nanoparticles (by coating), and synthesis of nanoparticles (by TiCl₄ treatment). The steps of all surface modifications are shown in Fig. 3.2.

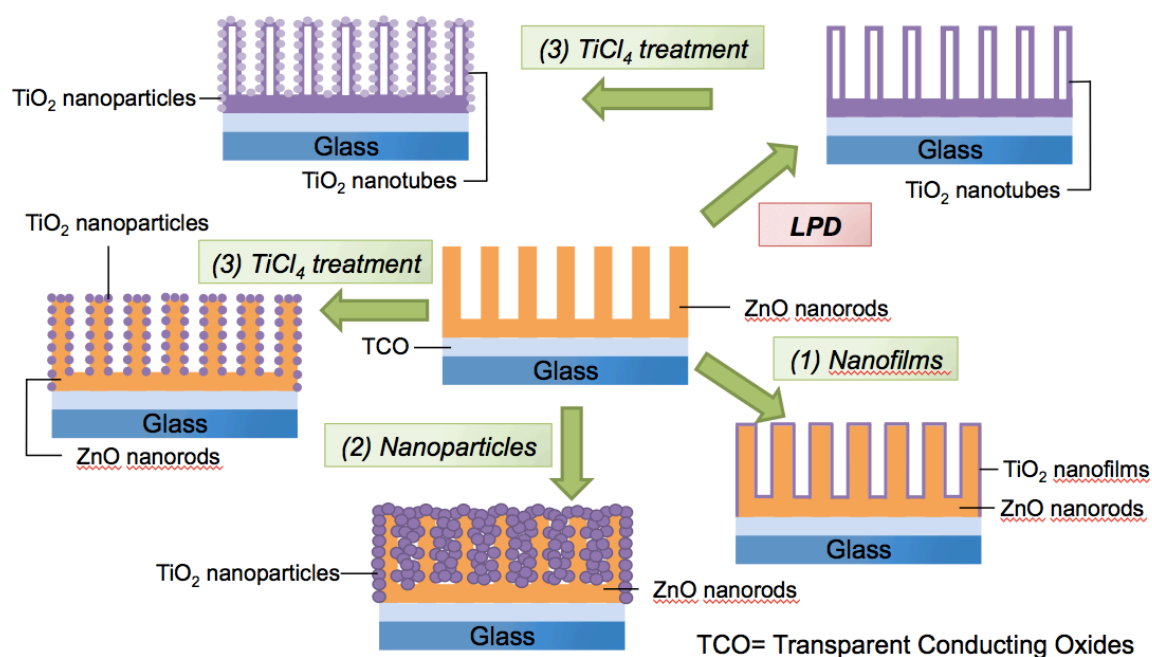


Fig. 3.2 Steps of surface modification.

3.2.1 Addition of TiO₂ Nanofilms on ZnO Surfaces

Precursor solutions for TiO₂ nanofilms were prepared by dissolving titanium (IV) butoxide in a solvent. The solvent of 2-propanol (2 ml) was stirred at room temperature. Then, titanium (IV) butoxide (0.1716 ml) was added into the above solution and the mixed solution was stirred continuously. Before addition of nanofilms, the glass side of the substrate was covered by protective tape to prevent the creation of nanofilms on this side. After blending, the precursor solution was coated onto the surface of ZnO nanorod arrays by immersion for 5 min. The cover tape was taken out after the dryness of the TiO₂ nanofilms.

3.2.2 Addition of TiO₂ Nanoparticles on ZnO Surfaces

TiO₂ nanoparticles were coated onto ZnO templates by the squeegee technique. The undesired area on substrate for adding TiO₂ nanoparticles was covered by protective tape. The nanoparticles were added to the margin of substrate and spread onto ZnO surfaces uniformly by using a glass rod. After addition of TiO₂ nanoparticles, the coated substrates were dried in the air and the tape (which covered the unrequired area) was pulled out.

3.2.3 TiCl₄ Treatment

In order to deposit the nanoparticles onto the surface of the nanorods and nanotubes, the synthesis of TiO₂ nanoparticles was carried out. The nanoparticles were synthesized by TiCl₄ solution, so called TiCl₄ treatment. Reaction of TiCl₄ with water to produce TiO₂ was highly exothermic and violent, which occurred suddenly. Before the addition of TiCl₄, the container with distilled water was kept in ice bath to cool water to 0-5 °C. A TiCl₄ (0.09 M in 20% HCl, 13 µl) solution was added into cold distilled water (7.5 ml). Then the mixed aqueous solution was heated to 70 °C with a hot plate. When the temperature of precursor solution reached the set point, TiO₂ nanotubes on substrates were immersed into the solution for 30 min and the substrates were posed vertically with the container bottoms. For the treatment of ZnO nanorods, the rods were treated with the precursor solution in the same conditions as described above, but the reaction time was change from 30 min to only 1 min, to protect the dissolution of ZnO rods. After immersion, the obtained substrates were rinsed with ethanol and dried.

3.3 Characterizations of Metal Oxide Nanowires

ZnO nanorods and TiO₂ nanowires were characterized by a scanning electron microscope (SEM, JEOL JSM-6610LV) and a field emission scanning electron microscope (FE-SEM, Hitachi SU6600, at Kyoto University) to observe morphology and structure. The element signatures of the nanorods and nanotubes were investigated by using energy-dispersive X-ray (EDX, Hitachi SU6600, at Kyoto University). The crystalline structure and average crystal sizes of prepared nanowires will be determined by an X-ray diffractometer (XRD, Bruker D8 Advance, at NSTDA).

3.4 Fabrication of Organic/Inorganic Hybrid Solar Cells

FTO substrates with ZnO nanorods (no heat treatment) or TiO₂ nanowire arrays (calcination at 450 °C for 1 h) were used to form electron-transporting layers. Solution of blended PCBM and P3HT (1:0.8, w/w) in chlorobenzene (1 μ l) was spin-coated on the TiO₂ nanowire arrays to achieve an active layer. Subsequently, the prepared sample was thermal annealed at 150 °C for 6 min under dry environment. After the heat treatment, 10 nm of molybdenum trioxide (MoO₃), which served as buffer layer, was coated onto the blended polymer. Finally, 100 nm of silver (Ag), which was an anode, was deposited by thermal evaporation. An example of energy level of devices made of TiO₂ nanowires is shown in Fig. 3.3.

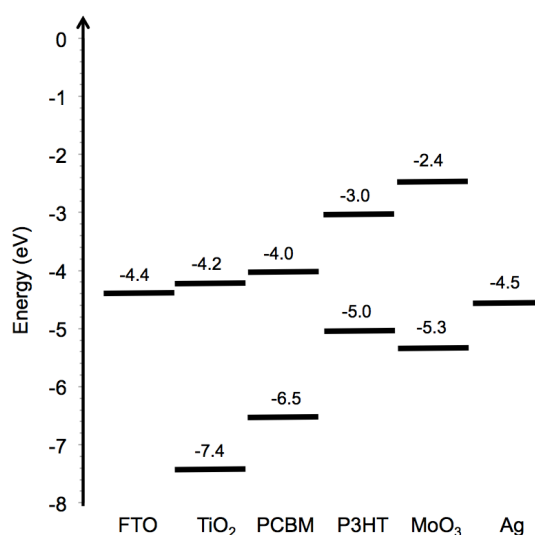


Fig. 3.3 Energy level of devices made of TiO₂ nanowires.

3.5 Photovoltaic Characterizations

Power conversion efficiency and photocurrent density-voltage (J - V) curves were measured under an ambient atmosphere and simulated solar light, AM 1.5, 100 mW/cm² by using a solar simulator with a xenon lamp (OTENTO-SUN III Solar Simulator, BUNKOU-KEIKI). The light intensity of illumination source was calibrated using a standard silicon photodiode (BS520BK, BUNKOU-KEIKI).

CHAPTER 4

RESULTS AND DISCUSSION

4.1 Effects of Preparation Conditions on Size and Morphology of ZnO Nanorods

4.1.1. Seed Layer

The ZnO nanorod arrays were grown by the hydrothermal method at 110 °C for 20 min. The morphological appearance of the ZnO nanorod arrays deposited on the glass substrates which were coated by seed layers with different thicknesses was observed by SEM. Fig. 4.1(a) shows ZnO nanorod arrays grown on 1 layer of seed thickness, ZnO nanorods have high density and small diameter of rods (~350 nm). The growth of ZnO nanorod arrays on 2 seed layers is shown in Fig. 4.1(b). With 2 seed layers, the ZnO nanorods seemed to be in more hexagonal structures and rod diameter was found to increase (~600 nm). As can be seen in Fig. 4.1(c), the diameter of ZnO nanorod arrays grown on 3 seed layers was the largest (~1 μ m) and the density of rods was lower than those of the other seed layers.

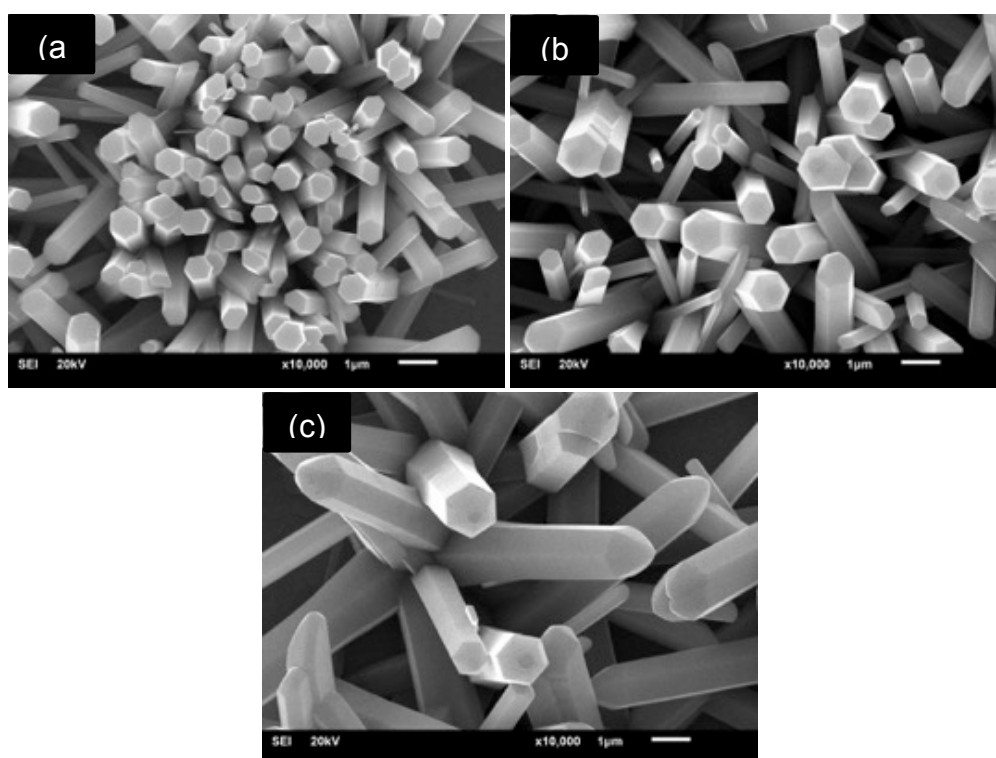


Fig. 4.1 SEM images of ZnO nanorod arrays grown on various seed layer thicknesses: (a) 1, (b) 2, and (c) 3 seed layer(s).

An XRD pattern of a cleaned substrate was shown in Fig. 4.2(a). Fig. 4.2(b) shows the XRD result of the thickness of 2 seed layers on the substrate after annealing. The XRD patterns of the ZnO nanorod arrays grown on coated substrate with 2 seed layers was observed as shown in Fig. 4.2(c). Many peaks in the pattern of ZnO nanorods on substrate were totally different from pristine substrate. Those were the characteristic peaks of ZnO in Wurtzite hexagonal structure.

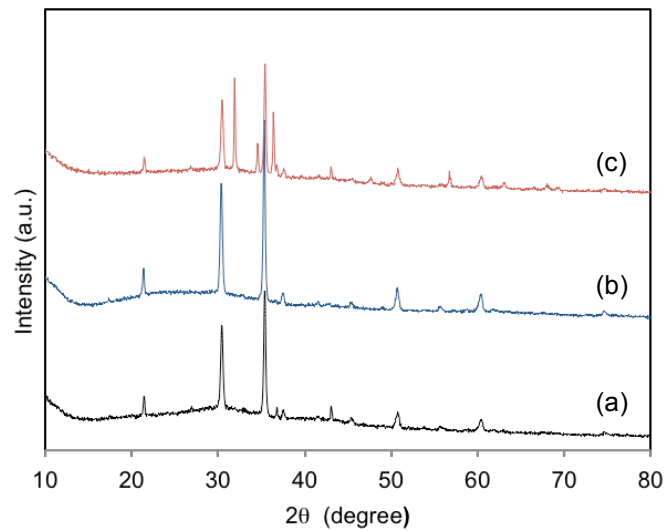


Fig. 4.2 XRD patterns of (a) cleaned substrate, (b) ZnO seeded on a substrate, and (c) ZnO nanorod arrays on a coated substrate.

It was found that the thinner seed layer had resulted in a higher density of ZnO nanorod arrays. This was the result of the nucleation sites on the surface of seed layer decreased when the thickness of seed layers increased. Moreover, the diameter size of nanorods relied on the particle size of seed layer, because the increase of seed layer thickness had an effect on the increase of particle size of seed layer. Therefore, the thickness of seed layer had a role for the diameter of ZnO nanorod arrays [20].

4.1.2 Deposition Time

Fig. 4.3 shows SEM images of ZnO nanorod arrays with different times of hydrothermal growth. The growth time in this work was varied from 10 min to 40 min and ZnO nanorod arrays were grown at 110 °C. It was found that diameter size of nanorods increased and the density of nanorods decreased with longer deposition time. The XRD patterns of ZnO nanorod arrays indicated in Wurtzite hexagonal structures, even though,

the deposition time changed (results not shown here). The similar effect of the reaction time for the growth of ZnO nanorods was also reported by other researchers [13, 48].

The first hour of hydrothermal growth was an initial period and very important for the ZnO nanorods, because of the highest supersaturation of the solution and the formation of nanocrystals on which the nanorods grew with the help of coated ZnO layers. Within the initial 20 min, the nanorod growth rate was very slow, after 20 min, the growth rate began as a fast step and observation of hexagonal ZnO nanorods was clear. The growth in radial direction was explained by kinetic studies that the nanorods tend to be short and wide with a fast step within the first hour [13]. Fig 4.3(a) shows the growth of nanorods for 10 min, ZnO nanorods has high density and small diameter of rods (<500 nm). As can be seen in Fig. 4.3 (d), the diameter of ZnO nanorod arrays grown for 40 min was the largest ($\sim 1\mu\text{m}$) and the density of rods was low. With extension of the reaction time, the nanocrystals grew bigger. The growth of nanorods was disturbed to go along the vertical line and resulted in the lower density of nanorods in longer deposition time [13]. All of ZnO nanorods under different growth time was shown in hexagonal structure. It implied that, the shape of nanorods was independent of the growth time [48]. Therefore, the deposition time was a parameter to control the diameter size and density of ZnO nanorods but no role on the hexagonal shape of ZnO nanorods.

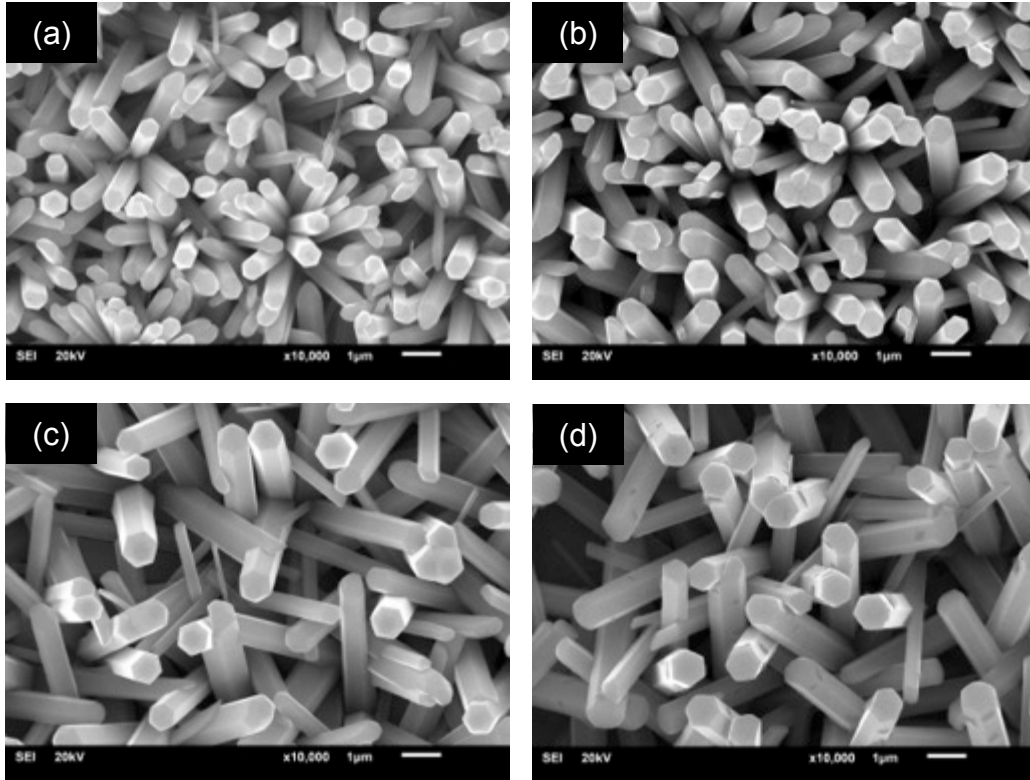


Fig. 4.3 SEM images of ZnO nanorod arrays grown on seeded substrates at different times of hydrothermal growth: (a) 10, (b) 20, (c) 30, and (d) 40 min.

4.1.3 Growth Temperature

The morphology of the ZnO nanorod arrays grown on the seeded substrates at different reaction temperatures is shown in Fig. 4.4. The growth temperature was varied in a range from 25 °C to 130 °C. As can be seen in Fig. 4.4(a), no nanorods of ZnO were observed at 25 °C, a possible reason was the formation of ZnO nanocrystalline grains as the principal process in this temperature. The reaction temperature of this result was below 30 °C according to previous work. It was reported by J. Zhao *et al.* (2006) [15] that the products fabricated at 30 °C were very short, showing a low rate of nanorod growth and the main process that occurred might have been the formation of ZnO crystalline grains. Fig. 4.4(b) shows the morphology of ZnO nanorods grown at 90 °C. The products were hexagonal nanorods but the top of that was tip-like [18]. As shown in Figs. 4.4(c) and 4.4(d), both obtained products at 110 °C and 130 °C were uniform hexagonal ZnO nanorod arrays. Their densities were high, because of small sizes of diameter. It was found that, at low growth temperature, the mobility and diffusion length of ions were restricted, which obstructed the ions to go around, and that caused the formation of large size nuclei [49].

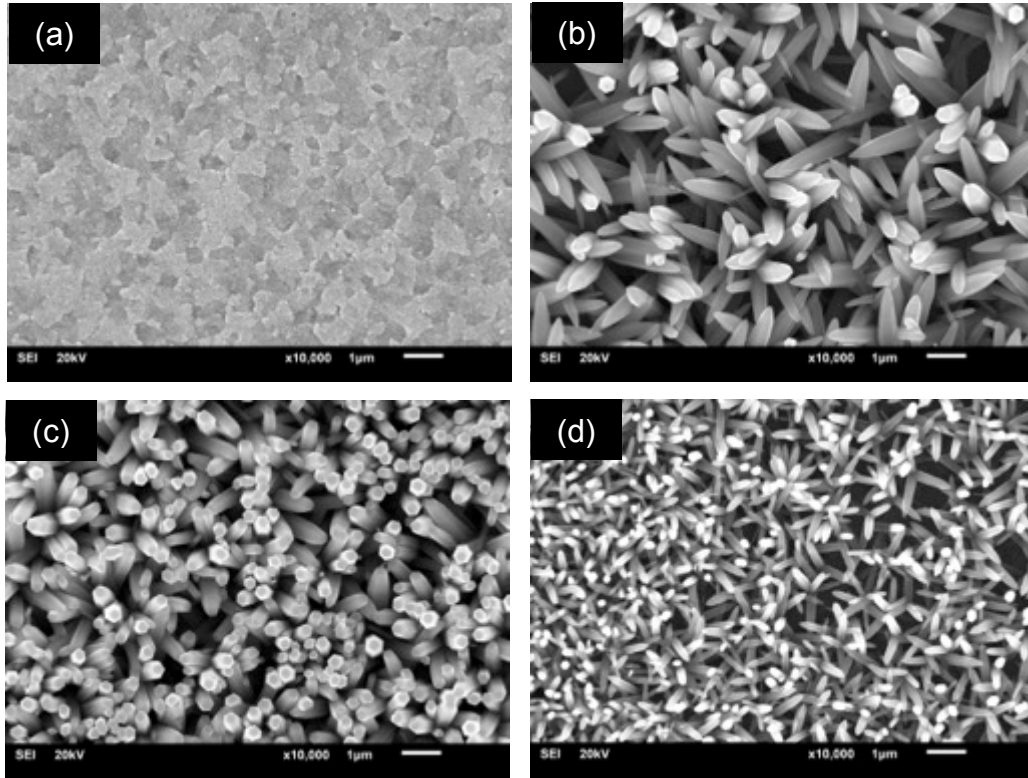


Fig. 4.4 SEM images of ZnO nanorod arrays grown on seeded substrates at different temperatures of hydrothermal growth: (a) 25, (b) 90, (c) 110, and (d) 130 °C.

In this work, when the growth temperature was increased from 90 °C to 130 °C, the size of the nanorods decreased and the rod density increased. However, M. Guo *et al.* (2005) [14] reported that the ZnO nanorod diameters increased with increasing the reaction temperature from 60 °C to 95 °C. The reason for unlike results might be the different range of growth temperature and reaction time. Therefore, it implied that the growth temperature had a significant role to control size and density of ZnO nanorod arrays.

4.1.4 Different Cooling Styles after Annealing Step

After the annealing step, it was found that the cooling style for the seeded substrate had an influence on the growth of the ZnO nanorods. A slow cooling style meant that the seeded substrates were cooled to room temperature in the furnace, which was different from the fast cooling style. The seeded substrates were taken out of the furnace to cool down in the air. As can be seen in Fig. 4.5, the density of ZnO nanorods grown on prepared substrate by fast cooling was higher than that prepared by slow cooling. It might be implied that during fast cooling, there was insufficient time to rearrange ions along the crystal planes having similar lattice match to decrease their high surface energy, while

slow cooling style, there was enough time to do that. Therefore, the prepared substrate by fast cooling, the nuclei were kept the same as that at annealing temperature, which caused the high density and particular growth of ZnO nanorods [15]. It could be concluded that the fast cooling style was a parameter to control the diameter size and density of ZnO nanorods.

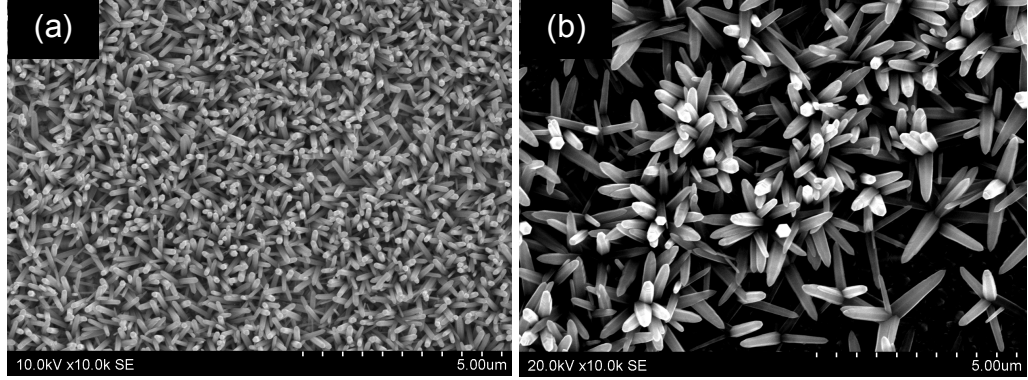


Fig. 4.5 SEM images of ZnO nanorods grown on with different cooling styles after the annealing step: (a) fast cooling style and (b) slow cooling style.

4.2 Photovoltaic Characterizations of Hybrid Photovoltaic Devices Made of ZnO Nanorods

The ZnO nanorod arrays with various seed layer thicknesses were applied as electron transporting layers in hybrid photovoltaic cells. The structure of cell was TCO/ZnO nanorods/PCBM/P3HT/ WO_3 /Ag, as shown in Fig. 4.6.

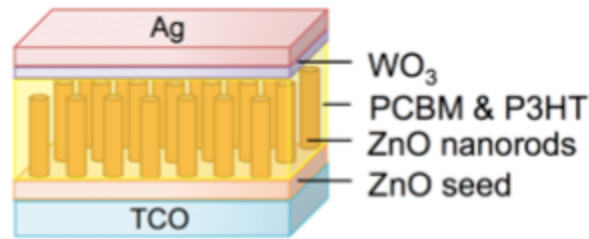


Fig. 4.6 Cell structure of hybrid photovoltaic cells made of ZnO nanorods.

Fig. 4.7 shows the J - V curves of hybrid photovoltaic cells made of ZnO nanorods grown on ZnO seeds at different seeding thicknesses. Table 4.1 shows the photovoltaic characteristic properties, i.e. short-circuit photocurrent density (J_{sc}), open-circuit voltage

(V_{oc}), fill factor (FF), and power conversion efficiency (PCE), of cells investigated. It was observed that ZnO nanorods grown on ZnO seed with 1 seed layer showed low PCE. Even the diameter of the cell was small, but the density of the nanorods was dense, so that the active PCBM:P3HT could not easily penetrate to the nanorods later. The PCE of the cells was found to increase by increasing seed layer to 2 layers. Even diameter of rods was larger which reduced the surface area, but the density of rods was suitable for the penetration of the active layer. Lastly, with 3 layers of seeding, the cell showed short circuit, because of too large diameter of nanorods with may stand over the active layer and contacted with Ag electrode. From this observation, it could be concluded that the suitable seed layers for ZnO seeding was 2 layers.

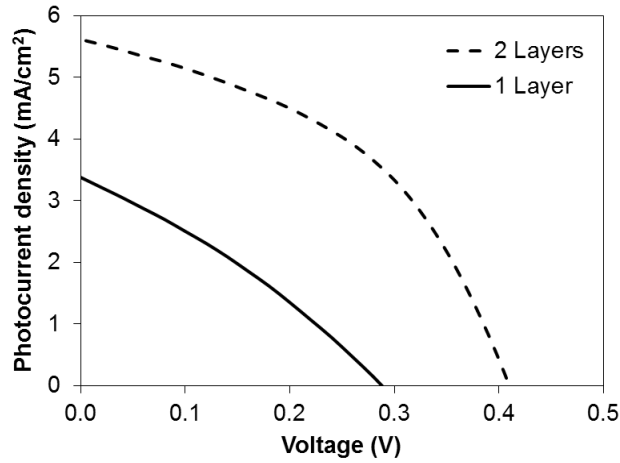


Fig. 4.7 J - V curves of hybrid photovoltaic cells made of ZnO nanorods grown on ZnO seeds at different seeding thickness.

Table 4.1 Photovoltaic characteristic properties of cells made of ZnO nanorods arrays grown on ZnO seeds at different seed layers.

Seed	J_{SC} (mA/cm ²)	V_{OC} (V)	FF	PCE (%)
1 layer	3.38	0.29	0.32	0.29
2 layers	5.62	0.41	0.44	1.02
3 layers	n/a	n/a	n/a	n/a

4.3 Fabrication of TiO₂ Nanotubes Using ZnO Nanorods as Templates

Fig. 4.8 shows SEM images in the top view of ZnO nanorods as templates and TiO₂ nanotubes, which were prepared by the liquid phase deposition method. ZnO nanorod arrays grown on 2 ZnO seed layers were observed and their diameter sizes were less than 50 nm. The morphology of TiO₂ nanotubes deposited on ZnO nanorod templates is shown in Fig. 4.8(b). The dissolution of ZnO templates and the deposition of TiO₂ nanotubes occurred at the same time. Therefore, the removal rate of ZnO templates had an influence to control the formation of TiO₂ nanotubes such as diameter, density and length. Some the end-closed TiO₂ nanotubes were broken during the preparation for SEM analysis, which could be showed the inside of end-capped nanotubes [4]. The TiO₂ nanotubes had inside diameter of ~50 nm, which was similar size with ZnO core, and outside diameter of ~100 nm. The density of TiO₂ naotubes was lower than the templates due to rate of ZnO dissolution.

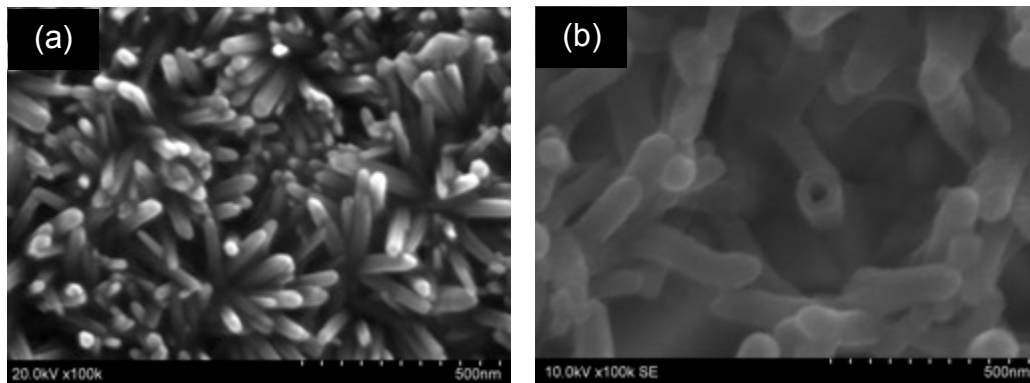


Fig. 4.8 SEM images of (a) ZnO nanorods as templates for producing (b) TiO₂ nanotubes.

Fig. 4.9 shows EDX spectra of ZnO nanorods and TiO₂ nanotubes. As can be seen in the figure, after the formation of the TiO₂ nanotubes, the ZnO nanorods were removed completely through selective etching. It was found that the element of zinc is only shown in Fig 4.9(a). Fig 4.9(b) shows the remaining elements after the deposition of the TiO₂ nanotubes. The figure shows that there was no zinc.

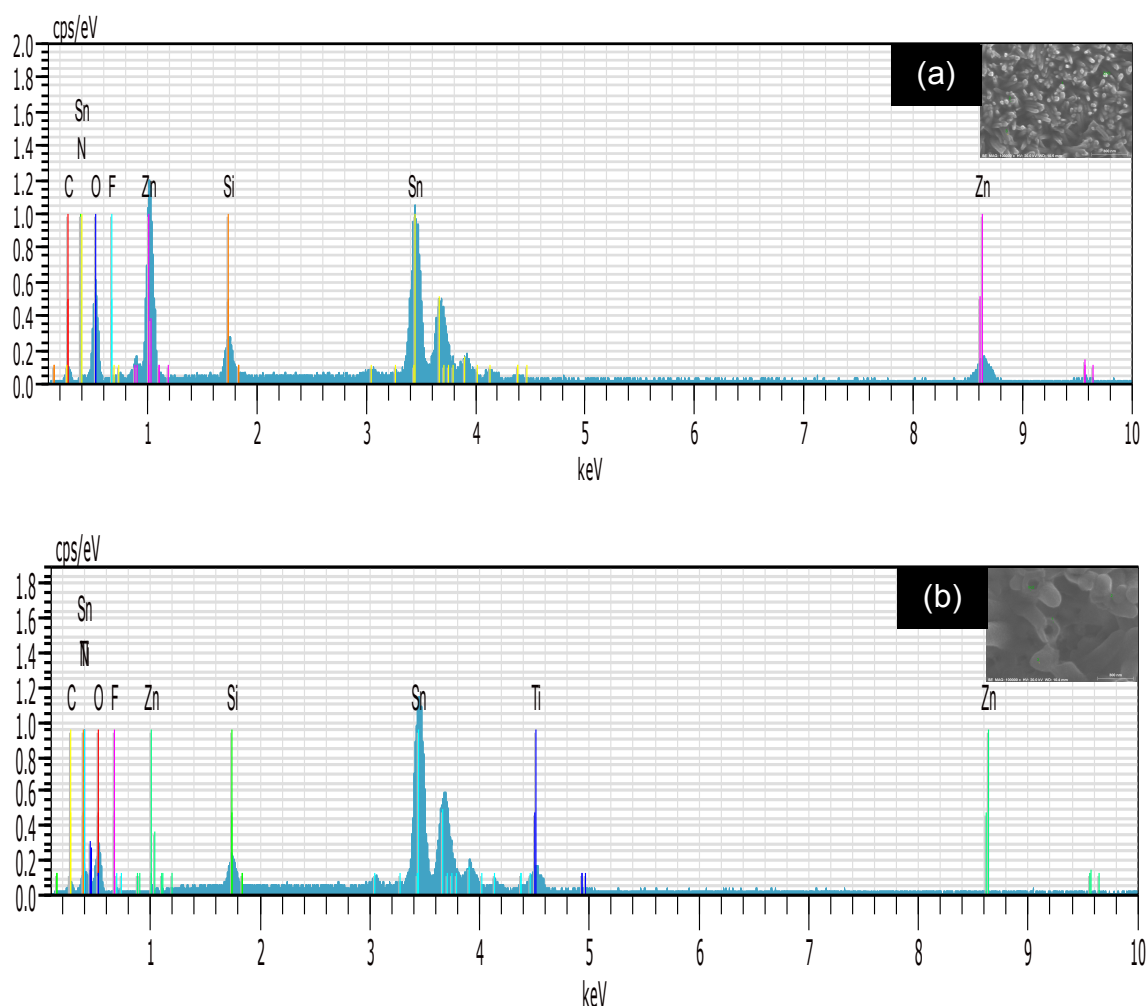


Fig. 4.9 EDX spectra of (a) ZnO nanorods as templates for producing (b) TiO₂ nanotubes.

4.4 Surface Modifications of Metal Oxides Nanowires

The ZnO nanorods templates were grown on 2 seed layers by the hydrothermal method with a growth temperature of 110 °C and a reaction time of 20 min. According to the methodology and results above, as can be seen in Fig. 4.10 (a), unmodified ZnO nanorods showed in Wurtzite hexagonal structures obviously and rod diameter was small (~50 nm). The length of nanorods was in range of 200-250 nm, as shown in Fig. 4.10(b).

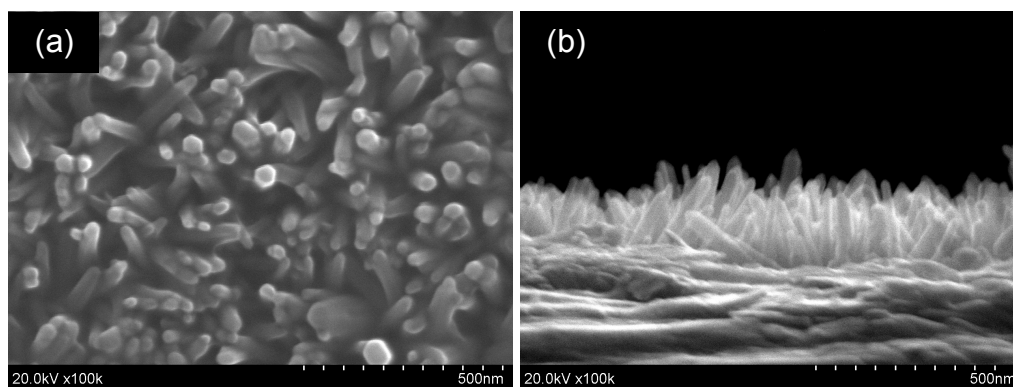


Fig. 4.10 SEM images of unmodified ZnO nanorod arrays in (a) top view and (b) cross-sectional view.

TiO₂ nanotubes were fabricated using ZnO nanorods as templates. ZnO nanorods and TiO₂ nanotubes were treated by different methods to modify their surface areas. The morphology of metal oxides with different surface modifications is shown in Fig. 4.11. The solution as precursor of TiO₂ nanofilms (NFs) were added onto ZnO nanorods (NRs), it was found that the thick nanofilms covered on ZnO surfaces obviously when compared with unmodified ZnO NRs as shown in Fig. 4.11(a) and (b). Fig. 4.12(a) shows the thick TiO₂ nanofilms in cross-sectional view. The films were thick at the same level throughout the substrate. Therefore film surfaces after addition of TiO₂ nanofilms become a uniform plane without any roughness of nanorods.

With modified surfaces by adding TiO₂ nanoparticles (NPs) by the squeegee technique, the experimental results show that all surfaces of the ZnO templates were covered by TiO₂ NPs. As can be seen in Figs. 4.11(c) and 4.12(b), the morphological appearances of obtained sample had significantly rough surface in the same plane that resulted from filling nanoparticles. They were added into the gap between nanorods and top surface of nanorods. It could be confirmed by EDX spectra, as shown in Fig 4.13. There was no zinc on the surface, which might imply that all ZnO nanorods had been covered by titanium from the addition of TiO₂ nanoparticles.

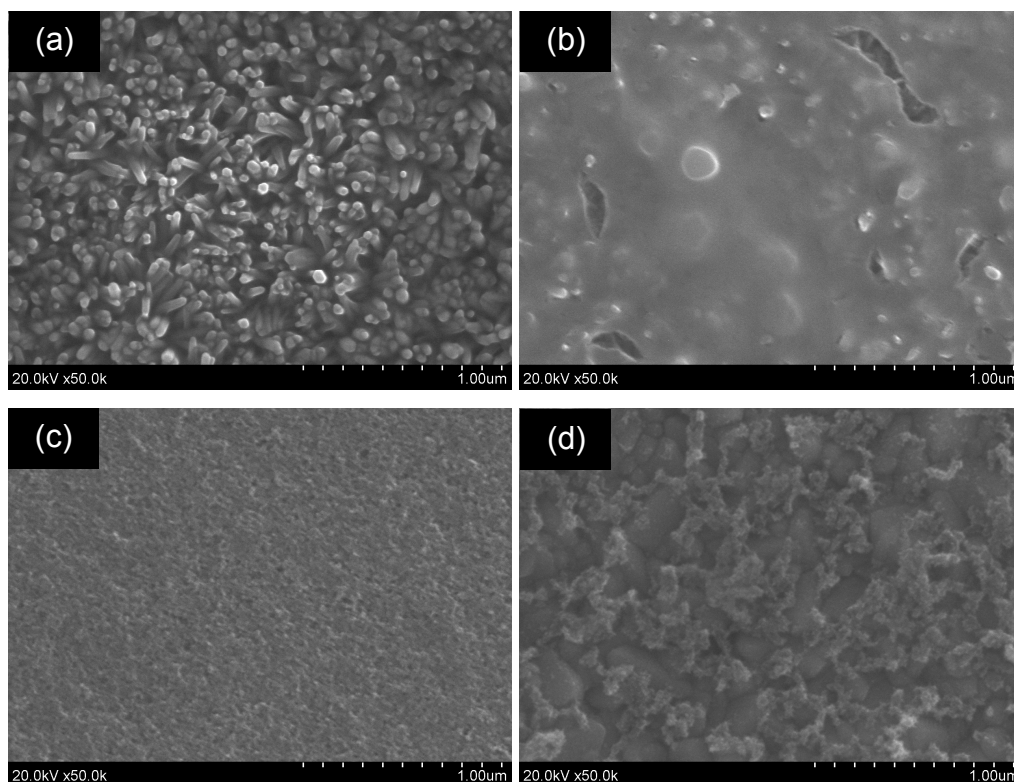


Fig. 4.11 SEM images of modified surface of ZnO nanorods: (a) unmodified ZnO nanorods, (b) TiO_2 nanofilms on ZnO surfaces, (c) TiO_2 nanoparticles on ZnO surfaces and (d) TiCl_4 treatment on ZnO nanorods.

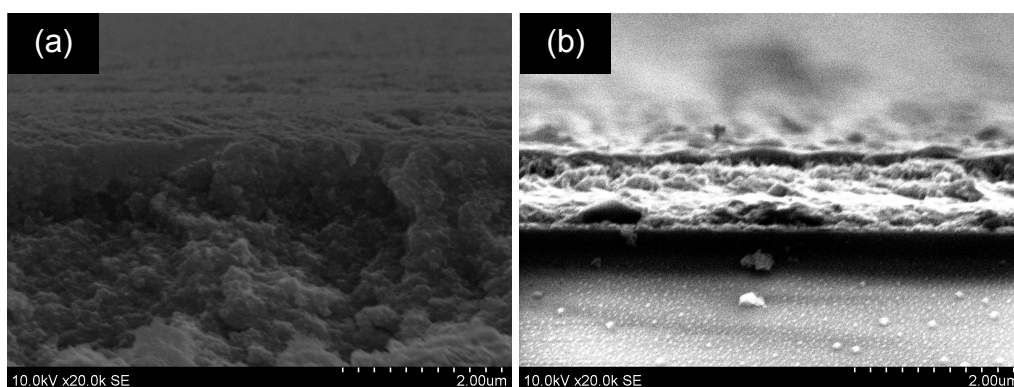


Fig. 4.12 SEM images in cross-sectional view of (a) TiO_2 nanofilms on ZnO surfaces and (b) TiO_2 nanoparticles on ZnO surfaces.

Fig. 4.11(d) shows ZnO NRs with the treatment of the surface by TiCl_4 . It was found that its surface was rougher than the surface of the addition of the nanoparticles

because the formation of nanoparticles by the TiCl_4 treatment had occurred on the entire surface of ZnO along the rod structure. The result was not demonstrated in rod structure directly, it might be implied that some ZnO NRs were removed by immersion in precursor solution because TiCl_4 solution had a component of acid, which might induce the dissolution of ZnO NRs. Although this TiCl_4 treatment was method to modify surface with nanoparticles, the concentration of precursor solution was low. Then the nanoparticles was formed in fewer amounts than addition of nanoparticle directly. They could not fill in the space of interface areas between nanorods totally. A possible way to decrease the removal of ZnO NRs during the surface treatment by TiCl_4 was reducing the time of immersion.

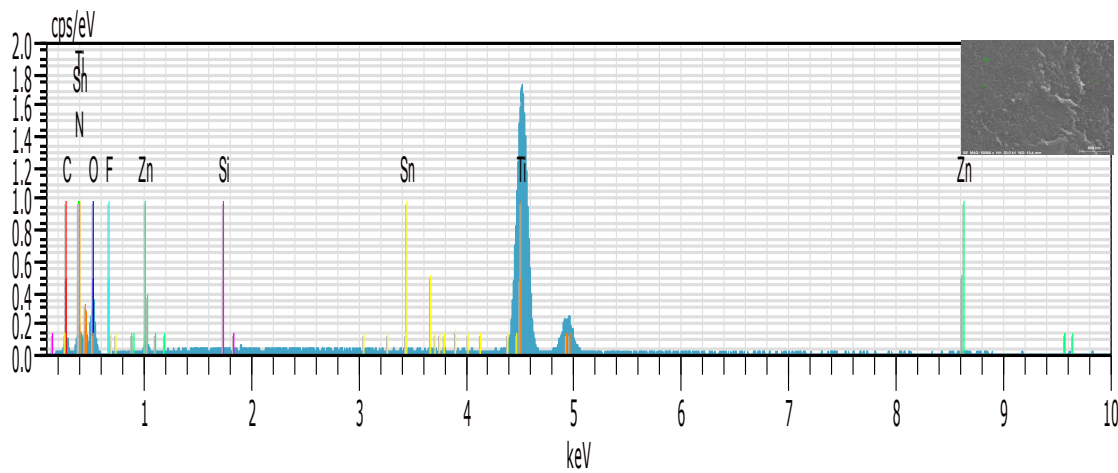


Fig. 4.13 EDX spectra of modified surface of ZnO by addition of TiO_2 nanoparticles.

The surface treatment on the TiO_2 nanotubes (NTs) by the TiCl_4 solution is shown in Fig 4.14(c). Their morphological appearances were different from unmodified TiO_2 nanotubes as shown in Figs 4.14(a) and 4.14(b). The TiO_2 nanotubes, which were prepared by liquid phase deposition using unmodified ZnO as template, were used to modify their surfaces with TiCl_4 treatment. It was found that the surface of the modified nanotubes with TiCl_4 has roughness because many nanoparticles were formed on the surface of nanotubes. TiCl_4 treatment led to the formation of TiO_2 nanoparticles on the surface of TiO_2 NTs, which resulted in the higher surface area to transport the electron for application in solar cells.

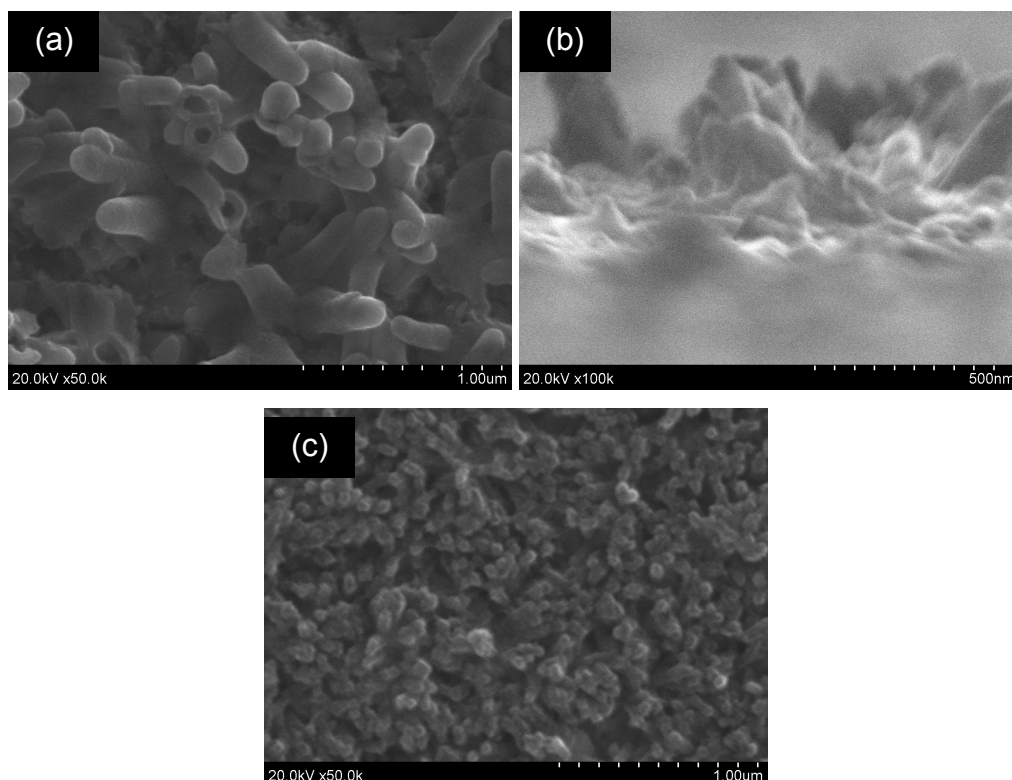


Fig. 4.14 SEM images of TiO₂ nanotubes with surface modifications: (a) unmodified TiO₂ nanotubes in top view, (b) unmodified TiO₂ nanotubes in cross-sectional view, and (c) TiCl₄ treatment on TiO₂ nanotubes.

4.5 Photovoltaic Characterizations of Hybrid Photovoltaic Devices Made of TiO₂ Nanowires

The unmodified and different modified surfaces of the metal oxides were served as electron transporting layers in the hybrid photovoltaic devices. The structure of the device was FTO/metal oxides/PCBM/P3HT/MoO₃/Ag, as shown in Fig 4.15.

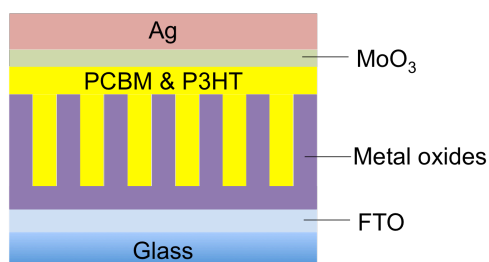


Fig. 4.15 Device structure of hybrid photovoltaic cell made of metal oxides.

4.5.1 Several Treatments

Fig. 4.16 shows the J-V curves of the hybrid photovoltaic cells made of unmodified and modified surfaces of metal oxides. Table 4.2 shows photovoltaic characteristic properties, i.e. short-circuit photocurrent density (J_{sc}), open-circuit voltage (V_{oc}), fill factor (FF), and power conversion efficiency (PCE), of cells were investigated. It was observed that the unmodified ZnO nanorods (NRs) had low PCE. Surface modifications with different methods, such as addition of TiO₂ nanoparticles (NPs), addition of TiO₂ nanofilms (NFs), and TiCl₄ treatment; were used to improve the cells efficiencies.

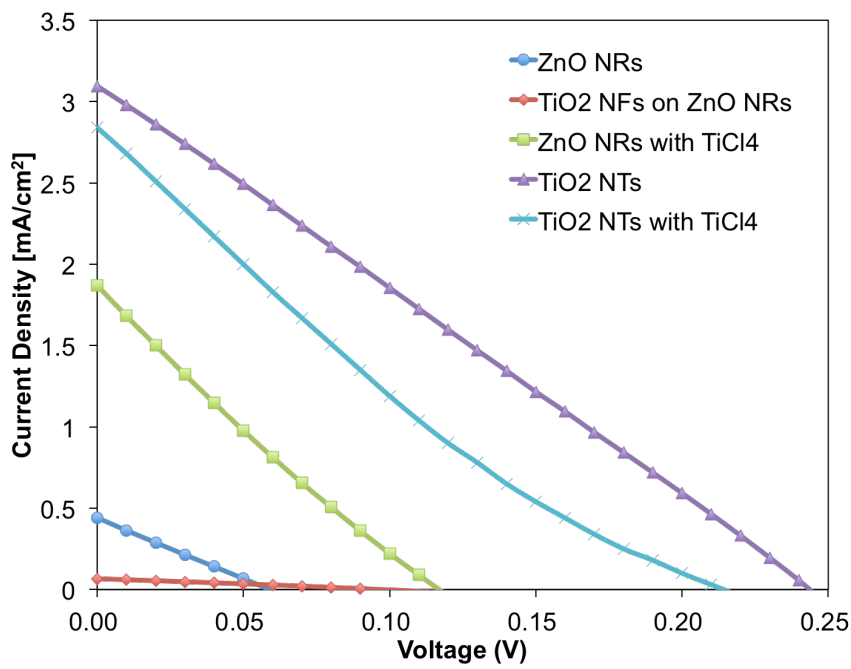


Fig. 4.16 J - V characteristics of hybrid photovoltaic devices fabricated from metal oxides.

Table 4.2 Photovoltaic characteristic properties of cells made of metal oxides

Samples	J_{SC} (mA/cm ²)	V_{OC} (V)	FF	PCE (%)
ZnO NRs	0.44	0.06	0.25	0.01
ZnO NRs with TiCl ₄ treatment	1.87	0.12	0.22	0.05
TiO ₂ NPs on ZnO NRs	n/a	n/a	n/a	n/a
TiO ₂ NFs on ZnO NRs	0.066	0.097	0.271	0.002
TiO ₂ NTs	3.10	0.24	0.25	0.19
TiO ₂ NTs with TiCl ₄ treatment	2.84	0.21	0.20	0.12

It was observed that unmodified ZnO NRs had low PCE (0.01 %). This PCE is not different from the literature reporting on the solar cells made of ZnO [5]. In the TiO₂ nanoparticles-coated ZnO nanorods (by the squeegee technique), short circuit was found in all the devices. This may because of the significantly rough surface of TiO₂ particle agglomeration, hence direct connection of undesired pathways.

The ZnO NRs modified by the TiCl₄ treatment demonstrated the higher PCE more than did the unmodified ZnO NRs, because the formation of the TiO₂ nanoparticles with TiCl₄ treatment increased the surface area and transporting pathways in NRs. J_{sc} of cells made of TiCl₄ treated ZnO NRs was more than 4 times higher than that of cells mad of unmodified ZnO NRs (1.87 and 0.44 mA/cm², respectively). However, the addition of TiO₂ NFs to cover ZnO surfaces showed very low PCE. This might be due to the formation of TiO₂ NFs being thick and the infiltration of nanofilms filling the voids between the nanorods, leading to a decrease in interface area between the active materials and the transporting layer.

The best PCE of the devices is 0.19%, which was obtained from the device made of TiO₂ NTs (formed using ZnO NRs as templates). This is because the nanotubes had higher interfacial surfaces than did the nanorods. Anatase TiO₂ was also reported to have higher electron conductivity than ZnO [4]. It caused the electron transports easily and induces to higher PCE. Although, TiCl₄ treatment on surface of TiO₂ NTs leading to increase of surface areas, TiO₂ NTs with modified surfaces by TiCl₄ had a lower PCE than TiO₂ NTs. Deconstruction of TiO₂ NTs after TiCl₄ treatment because of acidic condition is a problem of this treatment. Another possible reason was the nanoparticles blocked the voids between

the nanotubes partially [50]. It might be implied that the active PCBM:P3HT could not easily infiltrate to the bottom due to blocked voids by producing TiO_2 nanoparticles on the TiO_2 surfaces, leading to lower PCE than did the device made of unmodified TiO_2 nanotubes.

The plot of external quantum efficiency or incident photons to converted electrons (IPCE) ratio as a function of wavelength is illustrated in Fig. 6. The IPCE plot shows maximum value from TiO_2 nanotubes, it could be explained by increased charge carrier mobility after modified treatment.

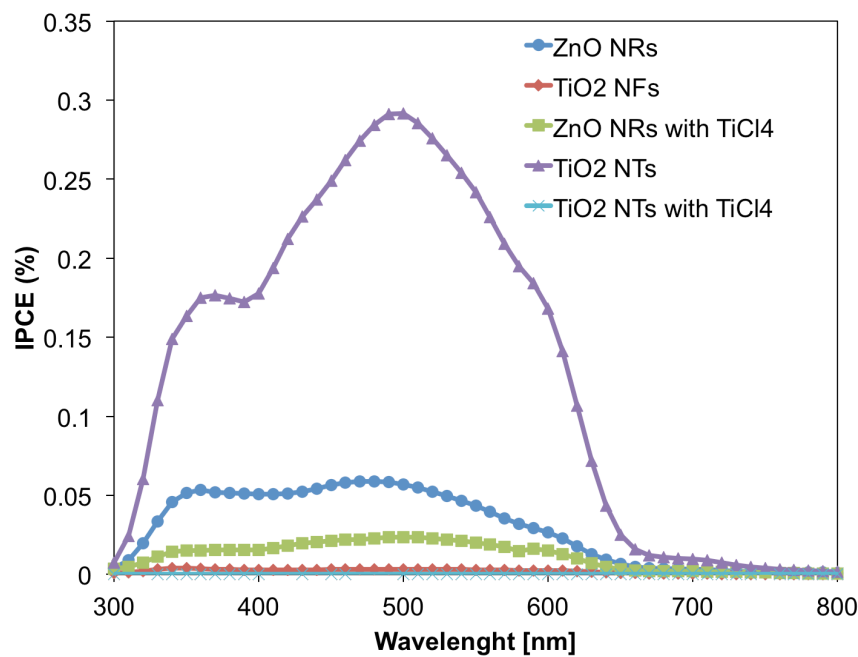


Fig. 4.17 IPCE characteristics of hybrid photovoltaic devices fabricated from metal oxides.

4.5.2 Improvement of Performance by Vacuum-assisted Coating

In the case of modified surfaces by TiO_2 nanofilms, the device which the photoactive layer was coated at atmospheric pressure showed very low PCE (0.002 %). To improve cell efficiencies, active layer was coated by vacuum-assisted coating technique. Fig. 4.18 shows SEM images of cells before and after improvement performance by vacuum-assisted coating. As can be seen in Figs. 4.18(a) and 4.18(b), cells made of TiO_2 nanofilms before improvement of active layer coating had thicker films than cells after improvement coating. The active layer in case of after improvement was not smooth plane

as shown in Fig. 4.18(b). However, cells made of TiO_2 nanotubes before and after improvement had the similar thicknesses of the active layer, which had a uniform plane without any roughness as, shown in Figs 4.18(c) and 4.18(d).

Fig. 4.19 shows the J - V curves of the devices with and without the improvement of active layer coatings. Table 4.3 shows photovoltaic characteristic properties, i.e. short-circuit photocurrent density (J_{sc}), open-circuit voltage (V_{oc}), fill factor (FF), and power conversion efficiency (PCE), of cells investigated. The efficiency of photovoltaic device based on TiO_2 nanofilms with vacuum-assisted coating of the active layer was more than 25 times higher than that of device made of nanofilms with active layer coating at atmosphere (0.05 and 0.002 %, respectively). Moreover cell made of TiO_2 nanotubes with vacuum-assisted coating had higher PCE than cell made of TiO_2 nanotubes without vacuum-assisted coating. V_{oc} and J_{sc} of cells made of TiO_2 nanotubes after improvement by vacuum-assisted coating were more than 2 times higher than that of cells before improvement. In vacuum system, the blended polymer could infiltrate to the bottom easier. This caused enhancement of the transporting pathways between the photoactive layers and electron transporting layers. Both of obtained results with vacuum-assisted coating had higher PCE. It might be implied that vacuum-assisted coating of active layer was a factor which had an influence on the electron transporting pathways. Therefore, the PCE of the devices increased after the improvement of the active layer coating.

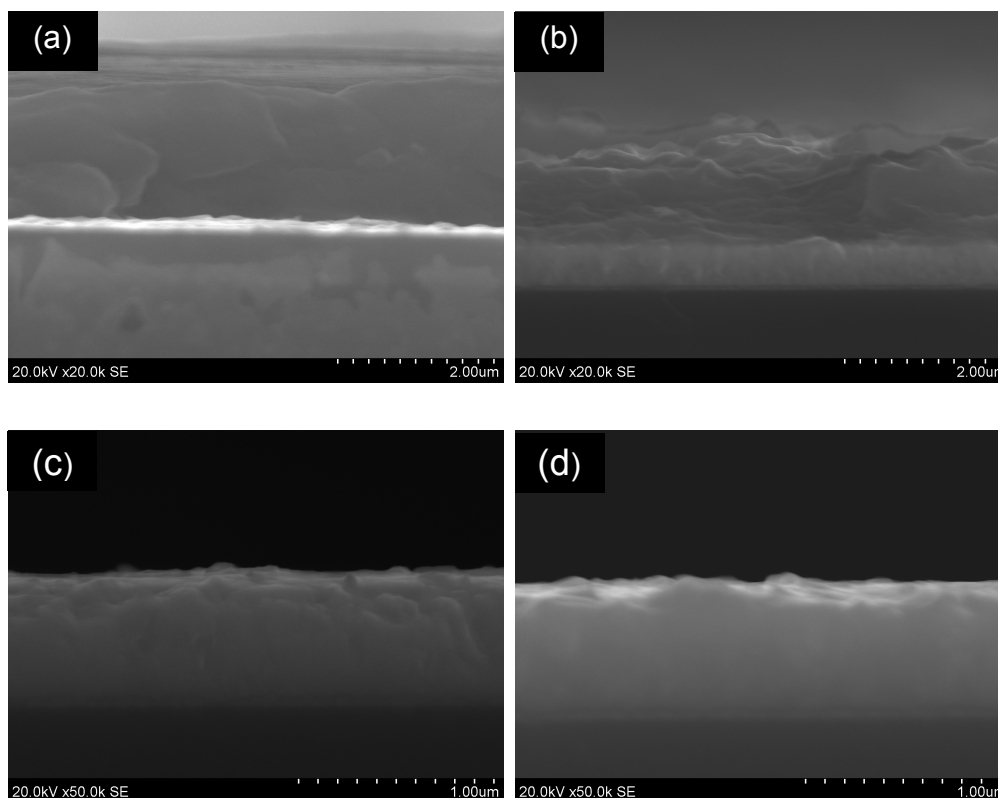


Fig. 4.18 SEM images of cells before and after improvement of performance by vacuum-assisted coating: (a) cell made of TiO_2 nanofilms before improvement, (b) cell made of TiO_2 nanofilms after improvement, (c) cell made of TiO_2 nanotubes before improvement, and (d) cell made of TiO_2 nanotubes after improvement.

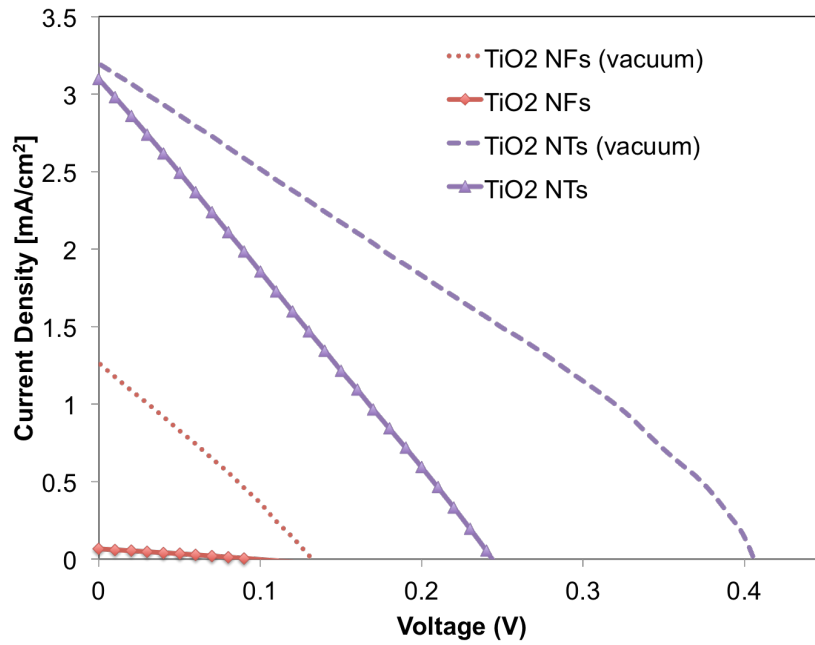


Fig. 4.19 J - V characteristics of hybrid photovoltaic devices fabricated from TiO₂ nanofilms and nanotubes with and without improvement of active layer coating.

Table 4.3 Photovoltaic characteristic properties of cells made of TiO₂ with and without vacuum-assisted coating of active layer

Samples	J_{SC} (mA/cm ²)	V_{OC} (V)	FF	PCE (%)
TiO ₂ NFs	0.066	0.097	0.271	0.002
TiO ₂ NFs (vacuum-assisted coating)	1.26	0.13	0.27	0.05
TiO ₂ NTs	3.10	0.24	0.25	0.19
TiO ₂ NTs (vacuum-assisted coating)	3.19	0.41	0.29	0.37

Moreover, coating of the active layer for 2 times (the first layer with vacuum-assisted coating and the second layer with normal coating) was studied to improve cell performance. As can be seen in Fig. 4.20, it was found that, the 2-time coating could further enhance the PCE of the devices due to the increase of J_{sc} (5 times).

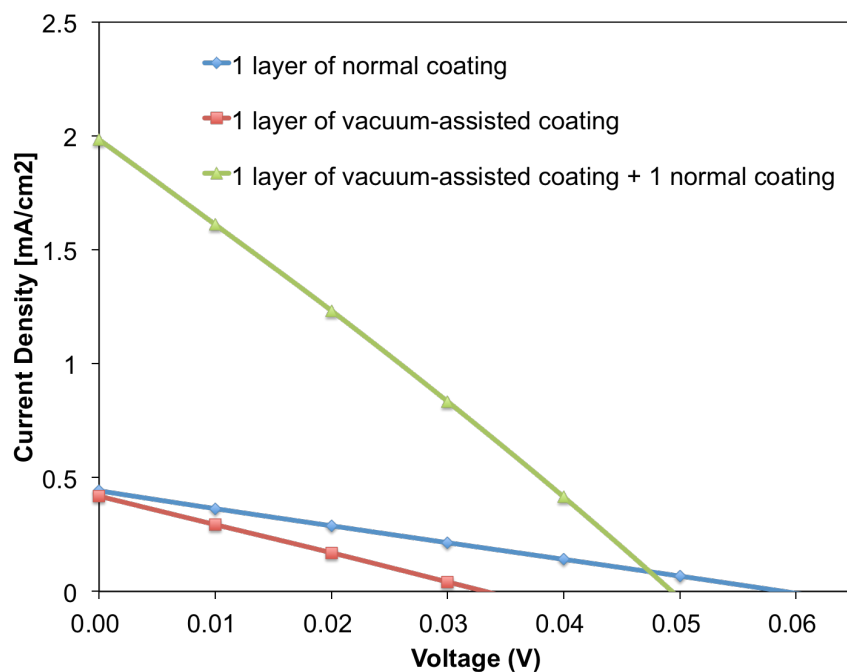


Fig. 4.20 J - V characteristics of hybrid photovoltaic devices fabricated from ZnO nanorods with and without vacuum-assisted coating of active layer.

Table 4.4 Photovoltaic characteristic properties of cells made of ZnO nanorods with and without vacuum-assisted coating of active layer

Samples	J_{sc} (mA/cm ²)	V_{oc} (V)	FF	PCE (%)
1 layer of normal coating	0.44	0.06	0.25	0.01
1 layer of vacuum-assisted coating	0.42	0.03	0.24	0.003
1 layer of vacuum-assisted coating + 1 layer of normal coating	1.98	0.05	0.26	0.03

CHAPTER 5

CONCLUSION

In this research, ZnO nanorods were synthesized by the hydrothermal method. SEM and XRD were used to characterize morphological appearance and crystallinity of nanorods, respectively.

The effects of preparation conditions on the size and morphology of the ZnO nanorods were studied. It was found that the size and morphology could be controlled by changes of seed layer, deposition time, growth temperature, and different cooling styles after annealing step. In particular, the diameter of ZnO nanorods increase with increasing thickness of seed layer, increasing deposition time, suitable temperature, and different cooling styles.

Various surface modifications on the ZnO nanorods, including the addition of a layer of TiO₂ nanofilm, TiCl₄ treatment, and synthesis of TiO₂ nanotubes (using ZnO nanorods as templates) were studied. TiCl₄ treatment on TiO₂ nanotubes was also carried out and compared. All 1D metal oxide nanoarrays were applied as an electron-transporting layer in hybrid photovoltaic cells. The devices made of TiO₂ nanotubes showed the highest PCE due to greater interface areas than these of the others. Nineteen-time improvement of PCE was achieved from TiO₂ nanotubes-based cells compared with unmodified ZnO nanorods-based cells.

For further improvement of PCE, optimization of the TiCl₄ treatment and the cell fabrication should be carried out.

REFERENCES

- 1 Ma, W., Yang, C., *et al.* (2005), Thermally stable, efficient polymer solar cells with nanoscale control of the interpenetrating network morphology, *Advanced Functional Materials*, **15**, pp. 1617-1622.
- 2 Li, G., Shrotriya, V., *et al.* (2005), High-efficiency solution processable polymer photovoltaic cells by self-organization of polymer blends, *Nature Materials*, **4**, pp. 864-868.
- 3 Reyes-Reyes, M., Kim, K., *et al.* (2005), High-efficiency photovoltaic devices based on annealed poly(3-hexylthiophene) and 1-(3-methoxycarbonyl)-propyl-1-phenyl-(6,6)C₆₁ blends, *Applied Physics Letters*, **87**, pp. 083506.
- 4 Rattanaavoravipa, T., Sagawa, T., *et al.* (2008), Photovoltaic performance of hybrid solar cell with TiO₂ nanotubes arrays fabricated through liquid deposition using ZnO template, *Solar Energy Materials & Solar Cells*, **92**, pp. 1445-1449.
- 5 Chuangchote, S., Sagawa, T., *et al.* (2011), Electrospun TiO₂ nanowires for hybrid photovoltaic cells, *Journal of Materials Research*, **26**, pp. 2316–2321.
- 6 Yeh, N. and Yeh, P. (2013), Organic solar cells: Their developments and potentials, *Renewable and Sustainable Energy Reviews*, **21**, pp. 421-431.
- 7 Malek, M. F., Sahdan, M. Z., *et al.* (2013), A novel fabrication of MEH-PPV/Al:ZnO nanorod arrays based ordered bulk heterojunction hybrid solar cells, *Applied Surface Science*, **275**, pp. 75-83.
- 8 Lee, J. and Jho, J. Y. (2011), Fabrication of highly ordered and vertically oriented TiO₂ nanotube arrays for ordered heterojunction polymer/inorganic hybrid solar cell, *Solar Energy Materials & Solar Cells*, **95**, pp. 3152-3156.
- 9 Ou, H.-H. and Lo, S.-L. (2007), Review of titania nanotubes synthesized via the hydrothermal treatment: Fabrication, modification, and application, *Separation and Purification Technology*, **58**, pp. 179-191.
- 10 Roy, P., Berger, S., *et al.* (2011), TiO₂ Nanotubes: Synthesis and Applications, *Angewandte Chemie International Edition*, **50**, pp. 2904 – 2939.
- 11 Lee, J.-H., Leu, I.-C., *et al.* (2005), Fabrication of aligned TiO₂ one-dimensional nanostructured arrays using a one-step templating solution approach, *The Journal of Physical Chemistry B*, **109**, pp. 13056-13059.

- 12 Ding, Y., Yang, C., *et al.* (2010), Photoelectrochemical activity of liquid phase deposited TiO_2 film for degradation of benzotriazole, *Journal of Hazardous Materials*, **175**, pp. 96-103.
- 13 Guo, M., Diao, P., *et al.* (2005), Hydrothermal growth of well-aligned ZnO nanorod arrays: Dependence of morphology and alignment ordering upon preparing conditions, *Journal of Solid State Chemistry*, **178**, pp. 1864-1873.
- 14 Guo, M., Diao, P., *et al.* (2005), The effect of hydrothermal growth temperature on preparation and photoelectrochemical performance of ZnO nanorod array films, *Journal of Solid State Chemistry*, **178**, pp. 3210-3215.
- 15 Zhao, J., Jin, Z.-G., *et al.* (2006), Growth and morphology of ZnO nanorods prepared from $\text{Zn}(\text{NO}_3)_2/\text{NaOH}$ solutions, *Journal of the European Ceramic Society*, **26**, pp. 3745-3752.
- 16 Yang, M., Yin, G., *et al.* (2008), Well-aligned ZnO rod arrays grown on glass substrate from aqueous solution, *Applied Surface Science*, **254**, pp. 2917-2921.
- 17 Ji, L.-W., Peng, S.-M., *et al.* (2009), Effect of seed layer on the growth of well-aligned ZnO nanowires, *Journal of Physics and Chemistry of Solids*, **70**, pp. 1359-1362.
- 18 Qin, Z., Liao, Q., *et al.* (2010), Effect of hydrothermal reaction temperature on growth, photoluminescence and photoelectrochemical properties of ZnO nanorod arrays, *Materials Chemistry and Physics*, **123**, pp. 811-815.
- 19 Bai, S.-N. and Wu, S.-C. (2011), Synthesis of ZnO nanowires by the hydrothermal method, using sol-gel prepared ZnO seed films, *Journal of Materials Science: Materials in Electronics*, **22**, pp. 339-344.
- 20 Ghayour, H., Rezaie, H. R., *et al.* (2011), The effect of seed layer thickness on alignment and morphology of ZnO nanorods, *Vacuum*, **86**, pp. 101-105.
- 21 Wahid, K. A., Lee, W. Y., *et al.* (2013), Effect of seed annealing temperature and growth duration on hydrothermal ZnO nanorod structures and their electrical characteristics, *Applied Surface Science*, **283**, pp. 629-635.
- 22 Deng, J., Wang, M., *et al.* (2014), Controlled synthesis of aligned ZnO nanowires and the application in CdSe-sensitized solar cells, *Journal of Alloys and Compounds*, **588**, pp. 399-405.

- 23 Wang, M., Xing, C., *et al.* (2014), Alignment-controlled hydrothermal growth of well-aligned ZnO nanorod arrays, *Journal of Physics and Chemistry of Solids*, **75**, pp. 808-817.
- 24 Dong, X., Yang, P., *et al.* (2014), Fabrication of ZnO nanorod arrays via electrospinning assisted hydrothermal method, *Materials Letters*, **135**, pp. 96-98.
- 25 Jitputti, J., Rattanaavoravipa, T., *et al.* (2009), Low temperature hydrothermal synthesis of monodispersed flower-like titanate nanosheets, *Catalysis Communications*, **10**, pp. 378-382.
- 26 Berhe, S. A., Nag, S., *et al.* (2013), Influence of seeding and bath conditions in hydrothermal growth of very thin (~20 nm) single-crystalline rutile TiO₂ nanorod films, *ACS Applied Materials & Interfaces*, **5**, pp. 1181-1185.
- 27 Wang, Z. J., Qu, S. C., *et al.* (2008), Hybrid bulk heterojunction solar cells from a blend of poly(3-hexylthiophene) and TiO₂ nanotubes, *Applied Surface Science*, **255**, pp. 1916–1920.
- 28 Liu, J., Wang, W., *et al.* (2008), Surface ligand effects in MEH-PPV/TiO₂ hybrid solar cells, *Solar Energy Materials & Solar Cells*, **92**, pp. 1403– 1409.
- 29 Wu, M.-C., Liao, H.-C., *et al.* (2009), Nanostructured polymer blends (P3HT/PMMA): Inorganic titania hybrid photovoltaic devices, *Solar Energy Materials & Solar Cells*, **93**, pp. 961–965.
- 30 Wu, M.-S., Tsai, C.-H., *et al.* (2011), Enhanced performance of dye-sensitized solar cell via surface modification of mesoporous TiO₂ photoanode with electrodeposited thin TiO₂ layer, *Electrochimica Acta*, **56**, pp. 8906–8911.
- 31 Kang, S. H., Kim, J.-Y., *et al.* (2007), Surface modification of stretched TiO₂ nanotubes for solid-state dye-sensitized solar cells, *The Journal of Physical Chemistry C*, **111**, pp. 9614-9623.
- 32 Choi, S. C., Lee, H. S., *et al.* (2012), Effects of light scattering TiO₂ surface-modified by dual oxide coating in dye-sensitized solar cells, *Advanced Powder Technology*, **23**, pp. 866–871.
- 33 Yu, K. and Chen, J. *et al.* (2009), Enhancing Solar Cell Efficiencies through 1-D Nanostructures, *Nanoscale Research Letters*, **4**, pp. 1-10.
- 34 Saunders, B. R. and Turner, M. L. (2008), Nanoparticle–polymer photovoltaic cells, *Advances in Colloid and Interface Science*, **138**, pp. 1-23.

- 35 OpenStax CNX (2011). An introduction to solar cell technology. Available online: <http://cnx.org/contents/dd0537a2-fb5d-439d-8feb-bf2e50656dae@1@1>.
- 36 Wright, M. and Uddin, A. (2012), Organic–inorganic hybrid solar cells: A comparative review, *Solar Energy Materials & Solar Cells*, **107**, pp. 87-111.
- 37 Heo, J. H., Im, S. H., *et al.* (2013), Efficient inorganic–organic hybrid heterojunction solar cells containing perovskite compound and polymeric hole conductors, *Nature Photonics*, **7**, pp. 486-491.
- 38 Günes, S. and Sariciftci, N. S. (2008), Hybrid solar cells, *Inorganica Chimica Acta*, **361**, pp. 581-588.
- 39 Zhou, Y., Eck, M., *et al.* (2011). Organic-inorganic hybrid solar cells: State of the art, challenges and perspectives, solar cells - new aspects and solutions, Prof. Leonid A. Kosyachenko (Ed.)
- 40 Günes, S., Neugebauer, H., *et al.* (2007), Conjugated polymer-based organic solar cells, *Chemical Reviews*, **107**, pp. 1324-1338.
- 41 Saunders, B. R. (2012), Hybrid polymer/nanoparticle solar cells: Preparation, principles and challenges, *Journal of Colloid and Interface Science*, **369**, pp. 1-15.
- 42 Liu, R. (2014), Hybrid organic/inorganic nanocomposites for photovoltaic cells, *Materials*, **7**, pp. 2747-2771.
- 43 Pang, Y. L., Lim, S., *et al.* (2014), A critical review on the recent progress of synthesizing techniques and fabrication of TiO₂-based nanotubes photocatalysts, *Applied Catalysis A: General*, **481**, pp. 127-142.
- 44 Liu, N., Chen, X., *et al.* (2014), A review on TiO₂-based nanotubes synthesized via hydrothermal method: Formation mechanism, structure modification, and photocatalytic applications, *Catalysis Today*, **225**, pp. 34-51.
- 45 Malvadkar, N., Dressick, W. J., *et al.* (2009), Liquid phase deposition of titania onto nanostructured poly-p-xylylene thin films, *Journal of Materials Chemistry*, **19**, pp. 4796-4804.
- 46 Gutiérrez-Tauste, D., Domènech, X., *et al.* (2008), Dopamine/TiO₂ hybrid thin films prepared by the liquid phase deposition method. *Thin Solid Films*, **516**, pp. 3831-3835.
- 47 OpenStax CNX (2009). “Liquid phase deposition”. Available online: <http://cnx.org/contents/1096167b-8518-4159-a88d-3b2ae4df6645@9.4@9.4>.

- 48 Polsongkram, D., Chamninok, P., *et al.* (2008), Effect of synthesis conditions on the growth of ZnO nanorods via hydrothermal method, *Physica B*, **403**, pp. 3713– 3717.
- 49 Xu, S., Lao, C.S., *et al.* (2008), Density-controlled growth of aligned ZnO nanowire arrays by seedless chemical approach on smooth surfaces, *Journal of Materials Research*, **23**, pp. 2072-2077.
- 50 Park, J.-H., Kim, J.-H., *et al.* (2012), Effects of TiCl_4 surface treatment on photoelectrochemical response of TiO_2 nanotube arrays, *Molecular Crystals and Liquid Crystals*, **568**, pp. 192-197.